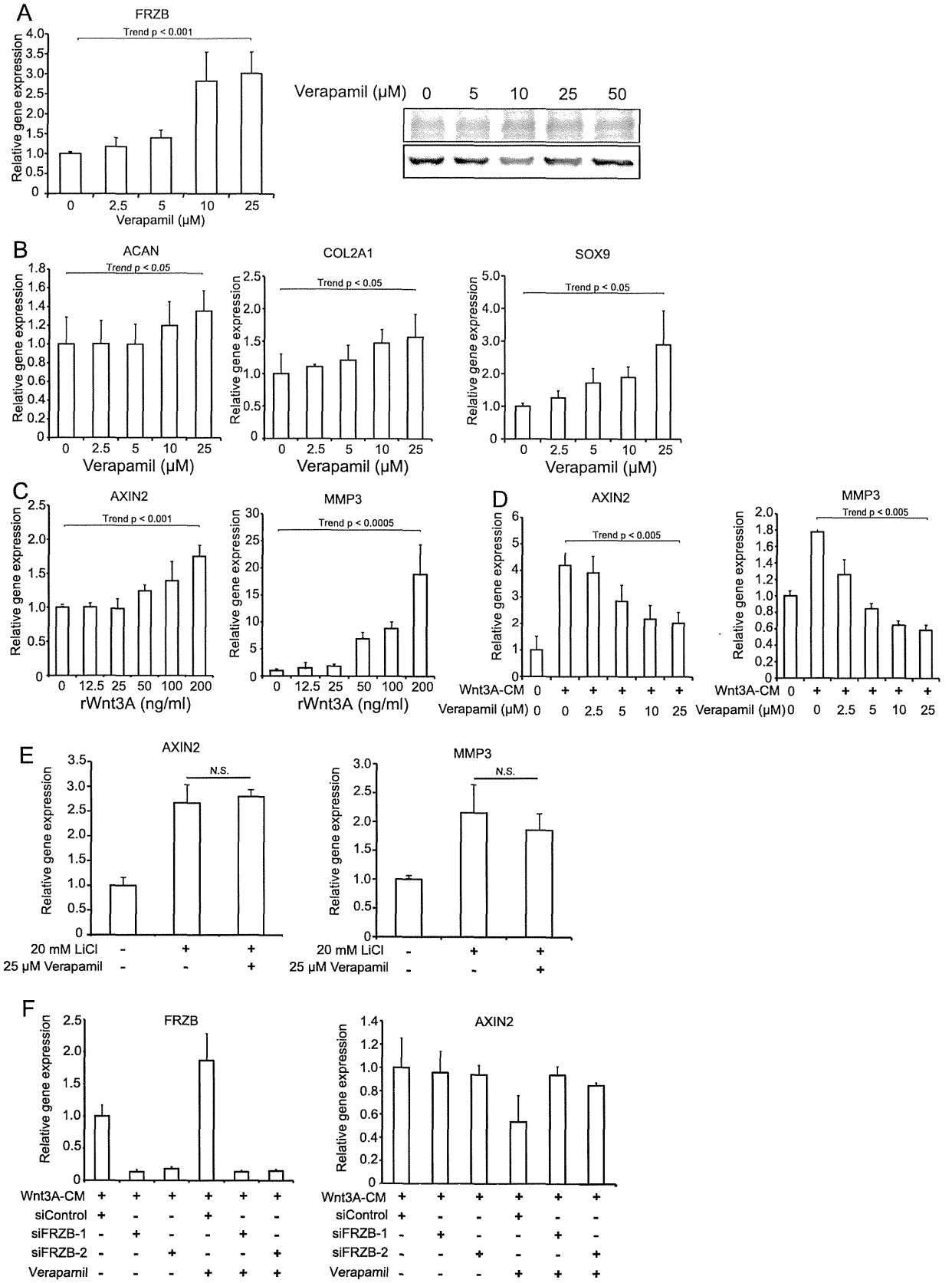
A
FRZB
Trend p < 0.001
Relative gene expression
Verapamil (μM)
Verapamil (μM) 0 5 10 25 50
B
ACAN
Trend p < 0.05
COL2A1
Trend p < 0.05
SOX9
Trend p < 0.05
C
AXIN2
Trend p < 0.001
rWnt3A (ng/ml)
MMP3
Trend p < 0.0005
rWnt3A (ng/ml)
D
AXIN2
Trend p < 0.005
MMP3
Trend p < 0.005
Wnt3A-CM
Verapamil (μM)
E
AXIN2
N.S.
MMP3
N.S.
20 mM LiCl
25 μM Verapamil
F
FRZB
AXIN2
Wnt3A-CM
siControl
siFRZB-1
siFRZB-2
Verapamil

Figure 2. Verapamil upregulates chondrogenic makers (*ACAN* encoding aggrecan, *COL2A1*, and *SOX9*) and downregulates Wnt-responsive *AXIN2* and *MMP3* in human osteoarthritic chondrocytes (OAC) cells. Expression levels of each mRNA are normalized to that without treatment. (A) Verapamil upregulates the native *FRZB* at the mRNA and protein levels in OAC cells ($n=3$). (B) Gene expressions of *ACAN*, *COL2A1*, and *SOX9* are increased by verapamil in 24 hrs. Purified Wnt3A protein increases *AXIN2* and *MMP3* mRNA expressions in 24 hrs (C), and verapamil inhibits the Wnt3A-induced gene expressions (D). (E) Verapamil does not suppress LiCl-induced *AXIN2* and *MMP3* expressions. (F) *FRZB* siRNAs (siFRZB-1 and siFRZB-2) cancel the effects of verapamil in Wnt3A-treated OAC cells. The mean and SEM ($n=3$) are indicated. *$p<0.05$ versus control by one-way ANOVA with Tukey's test.
doi:10.1371/journal.pone.0092699.g002

the ice-cold RIPA Lysis Buffer (Santa Cruz) supplemented with 0.1 mM dithiothreitol, 1 μg/ml leupeptin, 1 mM phenylmethylsulfonyl fluoride, and 1 μg/ml aprontinin. Whole cell lysates were separated on SDS-PAGE and transferred to a nitrocellulose membrane followed by immunoblotting with anti-β-catenin (BD Transduction Laboratories) and anti-β-actin (C4, Santa Cruz) antibodies.

Alcian blue staining

ATDC5 cells were supplied by the Riken BioResource Center (Tsukuba, Japan). ATDC5 cells were cultured in DMEM/F12 (a mixture of Dulbecco's modified Eagle's medium and Ham's F12 medium) (Sigma–Aldrich) supplemented with 5% fetal bovine serum (FBS, Thermo Scientific). ATDC5 cells were differentiated into chondrocytes with insulin-transferrin-selenite (ITS, Invitrogen) for two weeks, and were treated with Wnt3A-CM as well as with 0, 2.5, 5, 10, and 25 μM verapamil. After 72 hours, cells were fixed with methanol for 30 minutes at −20°C, and stained overnight with 0.5% Alcian Blue 8 GX (Sigma) in 1N HCl. For quantitative analyses, Alcian blue-stained cells were lysed in 200 μl of 6 M guanidine HCl for six hours at room temperature. The optical density of the extracted dye was measured at 630 nm using PowerScan 4 (DS Pharma Biomedical).

Immunofluorescence staining

OAC were fixed with 4% paraformaldehyde at room temperature. Coronal paraffin sections of proximal tibial growth plates were deparaffinized and hydrated in xylene. The specimens were then treated with a blocking buffer including 2% goat serum in 0.5% Triton-X100 for 60 minutes and incubated with mouse anti-β-catenin antibody (BD Transduction Laboratories, 1:500 dilutions for the cells and 1:100 dilutions for the sections) at 4 °C overnight. The specimens were incubated with goat anti-mouse fluorescein isothiocyanate (FITC) secondary antibody (1: 500 dilution) at room temperature for one hour. Finally, the specimens were mounted in VectaShield containing 1.5 μg/ml DAPI (Vector Laboratories, Peter-borough, UK) and visualized using IX71 (Olympus). The ratio of β-catenin-positive cells were automatically estimated by dividing FITC-positive cells by the number of DAPI-positive nuclei using MetaMorph (Molecular Device)

Explant culture of tibiae of mouse embryo

All animal studies were approved by the Animal Care and Use Committee of the Nagoya University and the animals were sacrificed under deep anesthesia, if necessary. maintained according to the guidelines for the care of laboratory animals of the Gifu International Institute of Biotechnology. Tibiae of wild type mouse embryo (E17.5) were dissected under the microscope, placed in a 24-well plate, and cultured in α-minimal essential medium (Invitrogen) supplemented with 0.2% bovine serum albumin, 1 mM β-glycerophosphate, and 50 μg/ml ascorbic acid. Embryonic tibiae were further treated with 20 mM LiCl or with 0, 25, and 50 μM verapamil for 10 days, then fixed in 10% formaldehyde in phosphate-buffered saline, demineralized with 0.5 M EDTA, and embedded in paraffin. Sections were stained with hematoxylin-eosin and Alcian blue. Hypertrophic cells were defined as having a length along the longitudinal axis greater than 10 μm under light microscopy. The numbers of hypertrophic chondrocytes were counted by two blinded observers and averaged.

In vivo generation of OA and its morphological evaluation

Wistar/ST rats were deeply anesthetized with an intraperitoneal injection of pentobarbital sodium (10 mg/ml×0.1 ml). Under sterile conditions, the right knee was induced to osteoarthritis by resection of the menisco-tibial ligament to destabilize medial meniscus (DMM surgery). Verapamil (50 μM) in 50 μl PBS was intraarticularly injected into the right knee each week. The skin and joint capsule on the left knee was incised (sham side). At four and eight weeks postoperatively, rats were sacrificed and tissue around the knees was fixed overnight in 4% paraformaldehyde at 4 °C, dehydrated, and embedded in paraffin. The sagittal sections were stained with Safranin O and Fast-green. OA progressions were graded according to the modified Mankin histologic score on both tibial and femoral sides of articular cartilages [21,22]. The modified Mankin score was a sum of the following seven parameters: articular cartilage structure, grades 0–11; tidemark duplication, grades 0–3; Safranin O staining, grades 0–8; fibro-cartilage, grades 0–2; chondrocyte clones in uncalcified cartilage, grades 0–2; hypertrophic chondrocytes in calcified cartilage, grades 0–2; and subchondral bone, grades 0–2. The grades of OA were estimated by two blinded observers and averaged.

Screening of verapamil-activated signaling pathways that facilitate upregulation of *FRZB*

For screening for involvement of other signaling molecules in verapamil-mediated activation of FRZB promoter, HCS-2/8 cells were co-transfected with the pGL4.10-*FRZB* and pCMV-SPORT6 Smurf1 (IMAGE clone 3660965, DNAFORM) or pCMV-SPORT6 Smurf2 (IMAGE clone 5345689, DNAFORM) and phRL-TK. At 24 hours after transfection, the cells were incubated for 24 additional hours in the presence of 50 μM of Verapamil with specific inhibitors of other signaling, SP600125 (JNK inhibitor), PD98059 (Erk inhibitor). Luciferase activity was measured using the Dual Luciferase Reporter Assay System (Promega)

Statistical analysis

Data are presented as the mean ± SEM. Statistical significance was determined either by unpaired t-test or one-way ANOVA followed by Tukey's post-hoc test. The Jonckheere-Terpstra trend test was used to assess dose responses, and is indicated by a letter 'trend' followed by a p value. Although one-way ANOVA gave more stringent values than the Jonckheere-Terpstra trend test,

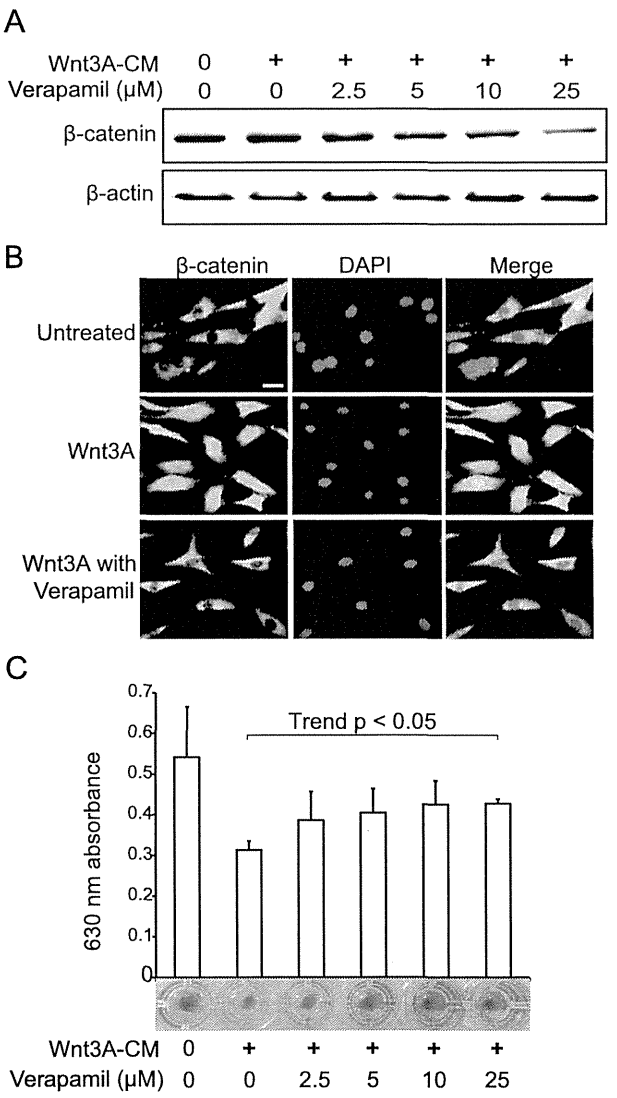

Figure 3. Verapamil suppresses Wnt-mediated protein expression and nuclear translocation of β-catenin in human osteoarthritic chondrocytes (OAC) cells, and verapamil rescues Wnt-induced loss of proteoglycans in chondrogenically differentiated ATDC5 cells. (A) Immunoblotting of β-catenin in OAC cells treated with Wnt3A-CM and verapamil for 72 hrs. (B) Immunofluorescence staining with anti-β-catenin antibody in OAC cells. Untreated cells (upper panels), cells treated with Wnt3A-CM alone (middle panels), and cells treated with Wnt3A-CM and 25 μM verapamil (lower panels) for 72 hours are stained with anti-β-catenin antibody (green, left panels) and DAPI (blue, middle panels). Wnt3A-induced nuclear localization of β-catenin is blocked by verapamil. Scale bar = 20 μm. (C) Alcian blue staining of ATDC5 cells that are differentiated to chondrocytes with ITS for two weeks. The cells are subsequently treated with Wnt3A-CM and verapamil for 72 hrs. Proteoglycans are quantified by measuring the optical density at 630 nm of the cell lysates. The mean and SEM (n = 3) are indicated. *p<0.05 versus control by one-way ANOVA with Tukey's test.
doi:10.1371/journal.pone.0092699.g003

one-way ANOVA was not suitable for estimating dose responses. P-values less than 0.05 were considered significant. The statistical analyses were performed with SPSS Statistics 21 (IBM).

Results

Verapamil enhances the *FRZB* promoter activity and reduces Wnt/β-catenin signaling activity

To identify a clinically applicable compound for OA, we transfected HCS-2/8 cells with either pGL4.10-*FRZB* to estimate the *FRZB* promoter activity or TOPFlash to estimate the Wnt/β-catenin activity. We searched for a compound that enhances the *FRZB* promoter and suppresses the Wnt/β-catenin activity among FDA-approved chemical compounds (Prestwick Chemical). These assays were repeated three times and we chose 41 best compounds. With the 41 compounds, we further repeated the assays three additional times. After the first and second rounds of screening, we chose 18 best compounds that consistently exhibited beneficial effects (data not shown). We next examined the dose-dependence by adding 0.5, 1, 5, 10, 50 μM of the 18 compounds. Among them, verapamil, a calcium channel blockers, showed the most consistent and promising dose-dependent activation of the *FRZB* promoter activity and can be used for a long time without major adverse effects (Figure 1A). We also found that verapamil suppressed the Wnt/β-catenin activity in a dose-dependent manner (Figure 1B). Verapamil is an L-type calcium channel blocker that has long been used for hypertension, angina pectoris, cardiac arrhythmia, and most recently cluster headache [23]. We also examined seven other calcium channel blockers (nifedipine, thioridazine, diltiazem, loperamide, perhexiline, nicardipine, felopdipine), but none had an effect (data not shown).

Verapamil upregulates native FRZB and induces expressions of chondrogenic genes in osteoarthritic chondrocyte (OAC) cells

In OA, breakdown of the extracellular matrix around chondrocytes leads to progressive destruction of articular structures [24]. To investigate the effect of verapamil on human OAC cells, we isolated OAC cells from patients with severe OA undergoing total knee replacement surgery. We first confirmed that verapamil upregulated the native FRZB at the mRNA and protein levels (Figure 2A). We screened signaling pathways that were potentially activated by verapamil to facilitate upregulation of FRZB, but found none (Figure S2).

Verapamil also upregulated mRNAs for *ACAN* encoding aggrecan, *COL2A1* encoding collagen type II α1, and *SOX9* encoding SRY-box 9 in a dose-dependent manner (Figure 2B). We next confirmed in OAC cells that Wnt3A upregulated *AXIN2* mRNA, a specific marker of Wnt/β-catenin signaling [25] and *MMP3* mRNA, a gene encoding catabolic metalloproteinase 3 (Figure 2C). As expected, verapamil suppressed *AXIN2* and *MMP3* in a dose-dependent manner (Figure 2D). We additionally observed that verapamil suppressed Wnt3A-mediated expression of total cellular β-catenin (Figure 3A), and nuclear translocation of β-catenin (Figure 3B).

LiCl is an inhibitor of Gsk3β and activates Wnt/β-catenin signaling. As expected, verapamil had no effects on LiCl-induced upregulations of *AXIN2* and *MMP3* in OAC cells (Figure 2E), whereas knocking down of *FRZB* cancelled the effects of verapamil (Figure 2F). These results underscored a notion that verapamil upregulates expression of FRZB and downregulates Wnt/β-catenin signaling in OAC cells.

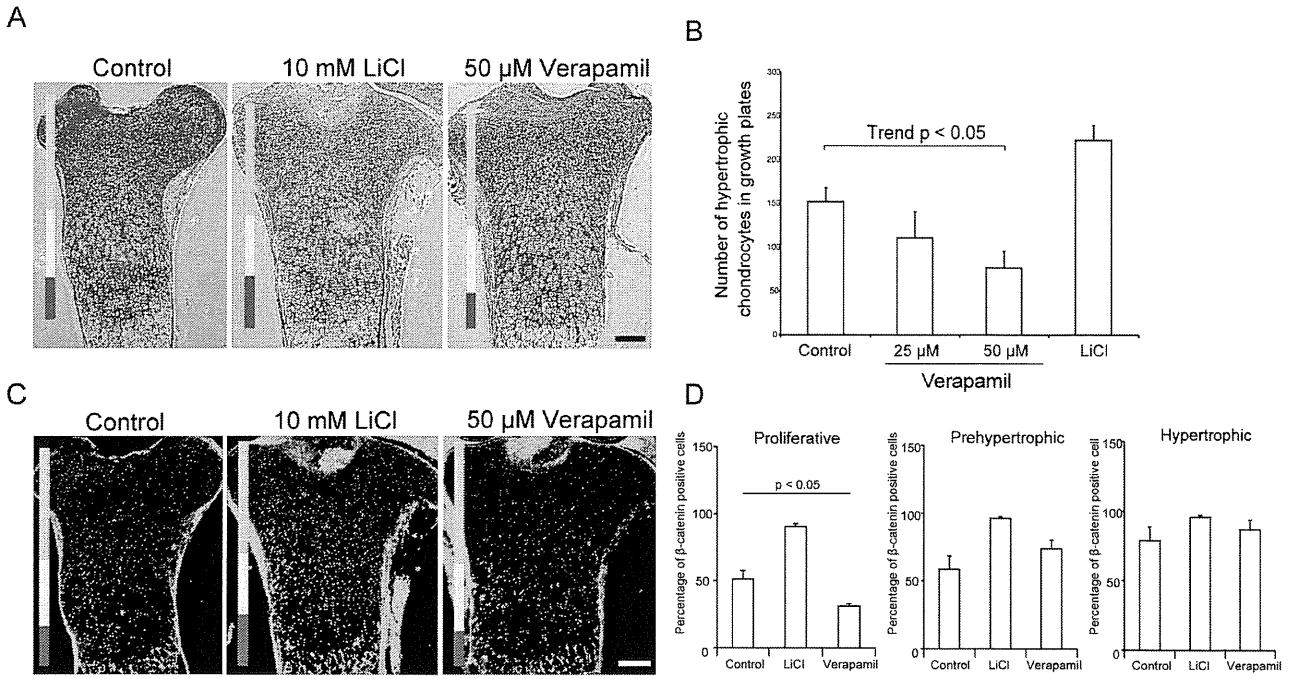

Figure 4. Verapamil suppresses hypertrophic differentiation of chondrocytes and β-catenin staining in growth plates in explanted mouse fetal tibiae on embryonic day 17.5. (A) Tibiae are cultured with LiCl or verapamil for 10 days, and coronal slices of paraffin sections are stained with Alcian blue combined with hematoxylin and eosin staining. Three layers of proliferative (green), prehypertrophic (yellow), and hypertrophic (red) zones are indicated by bars. Scale bar = 200 μm. (B) Verapamil suppresses the number of chondrocytes in the hypertrophic zone in (A). (C) Immunofluorescence with antibody against β-catenin in proximal tibiae of mouse embryo (E17.5). Color bars indicate layers as indicated in (A). Scale bar = 200 μm. (D) Verapamil suppresses the number of β-catenin-positive cells in the proliferative zone. The mean and SEM ($n = 3$) are indicated. *$p<0.05$ versus control by one-way ANOVA with Tukey's test.
doi:10.1371/journal.pone.0092699.g004

Verapamil rescues Wnt3A-induced degradation of proteoglycans in differentiated ATDC5 cells

Chondrocytes produce and maintain the cartilaginous matrix, which is mostly comprised of collagens and proteoglycans [7]. To investigate the effects of verapamil on degradation of proteoglycans, we performed Alcian blue staining to quantify acidic polysaccharides, such as glycosaminoglycans, in differentiated mouse chondrogenic ATDC5 cells. As OAC cells were not able to produce an appreciable amount of proteoglycans (data not shown), we used chondrogenically differentiated ATDC5 cells. We found that Wnt3A treatment induced loss of proteoglycans in ATDC5 cells and verapamil rescued the loss in a dose-dependent manner (Figure 3C).

Verapamil suppresses hypertrophic differentiation of chondrocytes in growth plates

Differentiation of chondrocytes including endochondral ossification is essential for embryonic skeletal growth, which has recently been demonstrated to be abnormally operational in development of OA [26]. Wnt/β-catenin signaling facilitates hypertrophic differentiation of chondrocytes in embryonic growth plates [27]. To investigate the effects of verapamil on hypertrophic differentiation of chondrocytes in growth plates, we cultured explanted mouse fetal tibiae with verapamil. We also treated the explanted tibiae with LiCl to confirm the responsiveness to Wnt/β-catenin. Verapamil had no gross effects on the metaphysis and diaphysis. Zonal analysis of the proximal growth plates showed that LiCl increased and verapamil decreased the height of the hypertrophic zone (Figure 4A). The numbers of hypertrophic chondrocytes counted by two blinded observers also underscored LiCl-mediated enhancement and verapamil-mediated suppression of the hypertrophic zone (Figure 4B). Immunostaining of β-catenin also showed that verapamil inhibited accumulation of β-catenin in growth plates, especially in the proliferative zone (Figures 4C and 4D). These results suggest that verapamil has an inhibitory effect on hypertrophic differentiation of chondrocytes in growth plates.

Verapamil ameliorates OA in a rat model

ure 5C). These results indicate that verapamil inhibits Wnt signaling and ameliorates progression of OA *in vivo*.

Discussion

In physiological endochondral ossification, chondrocytes become hypertrophic and remove the extracellular matrix proteins by expressing MMPs and ADMTSs. Chondrocytes finally die by apoptosis and are substituted by osteoblasts [28,29]. Recent studies disclose that OA follow a similar path to the physiological endochondral ossification: chondrocytes lose the stable phenotype and undergo terminal differentiations, as indicated by upregulation of marker genes for hypertrophy [26]. Wnt/β-catenin signaling pathway is known to drive endochondral ossifications by upregulating MMPs and ADAMTSs [30] in both physiological and pathological conditions [8]. Homeostasis of cartilage in adults is thus maintained by suppressed Wnt/β-catenin signaling, which is exemplified by the fact that FRZB functions as a natural brake to hypertrophic differentiation of chondrocytes [17]. Here we investigated the effects of verapamil on development and progression of OA, and revealed that verapamil (i) enhances

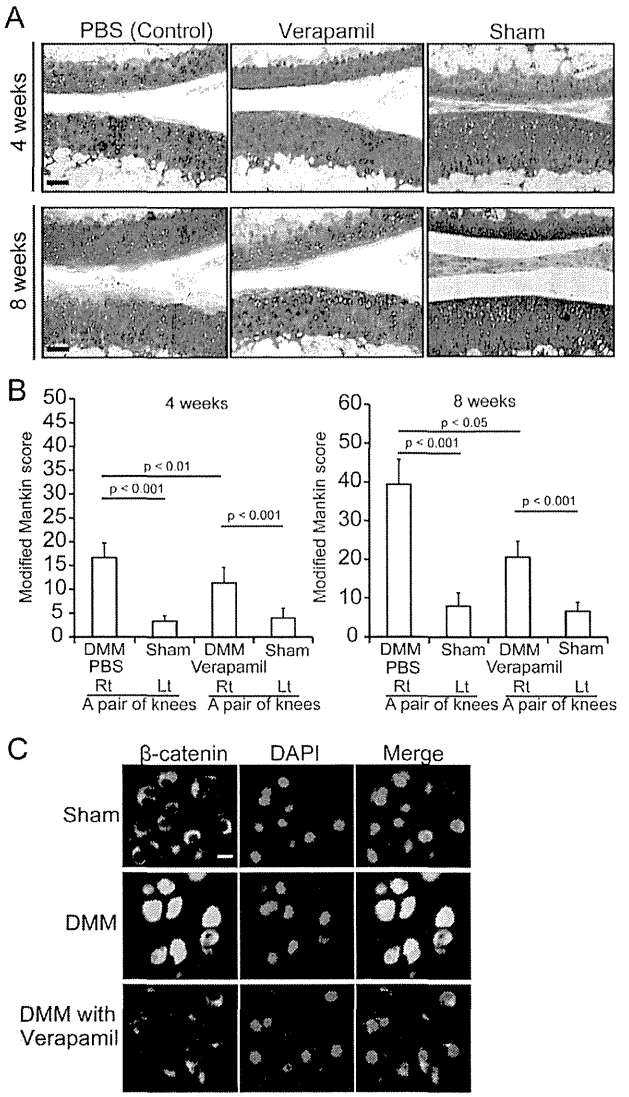

Figure 5. Verapamil prevents OA progression and β-catenin accumulation in rat DMM model. (A, B) DMM surgery induces mild OA phenotype in Wistar/ST rat and verapamil prevents OA progression. (A) Representative staining of knee joints with Safranin O and fast green. Scale bars = 200 μm. (B) Verapamil suppresses OA progressions evaluated by modified Mankin score at four and eight weeks after the surgery. Three rats in each group had DMM and sham surgeries in the right and left knees, respectively. Mean and SEM ($n = 3$) are indicated. (C) Immunofluorescence staining with anti-β-catenin antibody in rat articular cartilage. Articular chondrocytes at the weight-bearing sites are stained with anti-β-catenin antibody and DAPI. Nuclear translocation of β-catenin in DMM is blocked by verapamil. Scale bar = 20 μm.
doi:10.1371/journal.pone.0092699.g005

FRZB gene expression, (ii) inhibits Wnt/β-catenin signaling, (iii) suppresses ECM degradation, (iv) inhibits hypertrophic differentiation of chondrocytes, and (v) ameliorates OA model rats. We used up to 50 μM verapamil *in vitro* (Figure 1), *ex vivo* (Figure 4), and *in vivo* (Figure 5) without overt adverse effects, although the feasibility of intraarticular injection of 50 μM verapamil in clinical practice needs to be carefully validated.

In addition to FRZB, verapamil upregulates another chondrogenic key gene, *SOX9* (Figure 2B). SOX9 is a transcriptional factor that drives chondrogenic differentiation including upregulation of *COL2A1* [31], and is a physiological inhibitor against hypertrophic conversion of chondrocytes in growth plates [32]. Interestingly, physiological binding of SOX9 and β-catenin degrades both SOX9 and β-catenin, which indicates that activated Wnt/β-catenin degrades SOX9 and vice versa [33]. Verapamil is thus expected to increase the amount of SOX9 by suppressing Wnt/β-catenin. This mechanism is likely to account for the verapamil-mediated upregulation of *SOX9* transcripts (Figure 2B), because SOX9 protein upregulates expression of *SOX9* mRNA by forming a positive feedback loop [34].

As stated in the introduction, activation of Wnt/β-catenin worsens OA [7-11] and its inhibition ameliorates OA [12–14,17]. In contrast, however, constitutive inhibition of β-catenin in chondrocytes also leads to OA in mice [35]. Additionally, another Wnt antagonist, DKK1, promotes secretion of matrix proteinases in synovial fibroblasts and accelerates cartilage destruction [36]. These reports suggest that excessive suppression of Wnt/β-catenin may be rather deleterious in OA. The intraarticular administration of a high concentration of verapamil was likely to have suppressed Wnt/β-catenin signaling moderately and exerted beneficial effects in our rat model of OA.

The ATP-binding cassette (ABC) transporter exports hyaluronan to the extracellular matrix space [37] and hyaluronan is abnormally overproduced in OA cartilage [38]. As multidrug resistance (MDR) inhibitors including verapamil inhibits the ABC transporter [39], verapamil was intraarticularly injected in a rat OA model and verapamil indeed prevented abnormal production of hyaluronan and loss of aggrecan in osteoarthritic rat knees [40]. We observed a similar effect of verapamil on OA and have shown that the effects are mediated by upregulation of FRZB. Wnt/β-catenin signaling upregulates the ABC transporter in cerebral endothelium [41] and cancerous cells [42]. Although Wnt-mediated upregulation of the ABC transporter has not been reported in chondrocytes to our knowledge, suppression of the ABC transporter is likely to be another target of FRZB. As verapamil was approved as a class IV antiarrhythmic agent by FDA and has long been used without major adverse effects, verapamil holds promise as a therapeutic option for patients suffering from OA.

Supporting Information

Figure S1 Representative low magnification images of articular surfaces of rat knees after DMM surgery shown in Fig. 5A (boxed). Sections are stained with Safranin O and fast green. Scale bars = 500 μm.
(TIF)

Figure S2 Firefly luciferase activity for *FRZB* promoter in HCS cells treated with verapamil alone or in the presense of inhibitor of other signaling molecules. There are no significant difference between control and each group. Mean and SEM ($n = 8$) are indicated.
(EPS)

Acknowledgments

We would like to thank Dr. Masaharu Takigawa for providing HCS-2/8 cells.

Author Contributions

Conceived and designed the experiments: AT BO NI KO. Performed the experiments: AT. Analyzed the data: AT BO. Contributed reagents/materials/analysis tools: AT BO MI AM TS. Wrote the paper: AT BO KO.

References

1. Hunter DJ, Felson DT (2006) Osteoarthritis. BMJ 332: 639–642.
2. Lawrence RC, Felson DT, Helmick CG, Arnold LM, Choi H, et al. (2008) Estimates of the prevalence of arthritis and other rheumatic conditions in the United States. Part II. Arthritis Rheum 58: 26–35.
3. Kamekura S, Hoshi K, Shimoaka T, Chung U, Chikuda H, et al. (2005) Osteoarthritis development in novel experimental mouse models induced by knee joint instability. Osteoarthritis Cartilage 13: 632–641.
4. De Luca F, Barnes KM, Uyeda JA, De-Levi S, Abad V, et al. (2001) Regulation of growth plate chondrogenesis by bone morphogenetic protein-2. Endocrinology 142: 430–436.
5. Vortkamp A, Lee K, Lanske B, Segre GV, Kronenberg HM, et al. (1996) Regulation of rate of cartilage differentiation by Indian hedgehog and PTH-related protein. Science 273: 613–622.
6. Stewart AJ, Houston B, Farquharson C (2006) Elevated expression of hypoxia inducible factor-2alpha in terminally differentiating growth plate chondrocytes. J Cell Physiol 206: 435–440.
7. Yuasa T, Otani T, Koike T, Iwamoto M, Enomoto-Iwamoto M (2008) Wnt/beta-catenin signaling stimulates matrix catabolic genes and activity in articular chondrocytes: its possible role in joint degeneration. Lab Invest 88: 264–274.
8. Nalesso G, Sherwood J, Bertrand J, Pap T, Ramachandran M, et al. (2011) WNT-3A modulates articular chondrocyte phenotype by activating both canonical and noncanonical pathways. J Cell Biol 193: 551–564.
9. Thomas RS, Clarke AR, Duance VC, Blain EJ (2011) Effects of Wnt3A and mechanical load on cartilage chondrocyte homeostasis. Arthritis Res Ther 13: R203.
10. Zhu M, Tang D, Wu Q, Hao S, Chen M, et al. (2009) Activation of beta-catenin signaling in articular chondrocytes leads to osteoarthritis-like phenotype in adult beta-catenin conditional activation mice. J Bone Miner Res 24: 12–21.
11. Hwang SG, Yu SS, Ryu JH, Jeon HB, Yoo YJ, et al. (2005) Regulation of beta-catenin signaling and maintenance of chondrocyte differentiation by ubiquitin-independent proteasomal degradation of alpha-catenin. J Biol Chem 280: 12758–12765.
12. Lories RJ, Peeters J, Bakker A, Tylzanowski P, Derese I, et al. (2007) Articular cartilage and biomechanical properties of the long bones in Frzb-knockout mice. Arthritis Rheum 56: 4095–4103.
13. Lane NE, Nevitt MC, Lui LY, de Leon P, Corr M, et al. (2007) Wnt signaling antagonists are potential prognostic biomarkers for the progression of radiographic hip osteoarthritis in elderly Caucasian women. Arthritis Rheum 56: 3319–3325.
14. Chan BY, Fuller ES, Russell AK, Smith SM, Smith MM, et al. (2011) Increased chondrocyte sclerostin may protect against cartilage degradation in osteoarthritis. Osteoarthritis Cartilage 19: 874–885.
15. Hoang B, Moos M Jr, Vukicevic S, Luyten FP (1996) Primary structure and tissue distribution of FRZB, a novel protein related to Drosophila frizzled, suggest a role in skeletal morphogenesis. J Biol Chem 271: 26131–26137.
16. Loughlin J, Dowling B, Chapman K, Marcelline L, Mustafa Z, et al. (2004) Functional variants within the secreted frizzled-related protein 3 gene are associated with hip osteoarthritis in females. Proc Natl Acad Sci U S A 101: 9757–9762.
17. Leijten JC, Emons J, Sticht C, van Gool S, Decker E, et al. (2012) Gremlin 1, frizzled-related protein, and Dkk-1 are key regulators of human articular cartilage homeostasis. Arthritis Rheum 64: 3302–3312.
18. Abbott A (2002) Neurologists strike gold in drug screen effort. Nature 417: 109.
19. Bian Y, Masuda A, Matsuura T, Ito M, Okushin K, et al. (2009) Tannic acid facilitates expression of the polypyrimidine tract binding protein and alleviates deleterious inclusion of CHRNA1 exon P3A due to an hnRNP H-disrupting mutation in congenital myasthenic syndrome. Hum Mol Genet 18: 1229–1237.
20. Takigawa M, Tajima K, Pan HO, Enomoto M, Kinoshita A, et al. (1989) Establishment of a clonal human chondrosarcoma cell line with cartilage phenotypes. Cancer Res 49: 3996–4002.
21. Mankin HJ, Dorfman H, Lippiello L, Zarins A (1971) Biochemical and metabolic abnormalities in articular cartilage from osteo-arthritic human hips. II. Correlation of morphology with biochemical and metabolic data. J Bone Joint Surg Am 53: 523–537.
22. Furman BD, Strand J, Hembree WC, Ward BD, Guilak F, et al. (2007) Joint degeneration following closed intraarticular fracture in the mouse knee: a model of posttraumatic arthritis. J Orthop Res 25: 578–592.
23. Beck E, Sieber WJ, Trejo R (2005) Management of cluster headache. Am Fam Physician 71: 717–724.
24. Little CB, Fosang AJ (2010) Is cartilage matrix breakdown an appropriate therapeutic target in osteoarthritis–insights from studies of aggrecan and collagen proteolysis? Curr Drug Targets 11: 561–575.
25. Jho EH, Zhang T, Domon C, Joo CK, Freund JN, et al. (2002) Wnt/beta-catenin/Tcf signaling induces the transcription of Axin2, a negative regulator of the signaling pathway. Mol Cell Biol 22: 1172–1183.
26. Saito T, Fukai A, Mabuchi A, Ikeda T, Yano F, et al. (2010) Transcriptional regulation of endochondral ossification by HIF-2alpha during skeletal growth and osteoarthritis development. Nat Med 16: 678–686.
27. Hens JR, Wilson KM, Dann P, Chen X, Horowitz MC, et al. (2005) TOPGAL mice show that the canonical Wnt signaling pathway is active during bone development and growth and is activated by mechanical loading in vitro. J Bone Miner Res 20: 1103–1113.
28. Wang Y, Middleton F, Horton JA, Reichel L, Farnum CE, et al. (2004) Microarray analysis of proliferative and hypertrophic growth plate zones identifies differentiation markers and signal pathways. Bone 35: 1273–1293.
29. Inada M, Wang Y, Byrne MH, Rahman MU, Miyaura C, et al. (2004) Critical roles for collagenase-3 (Mmp13) in development of growth plate cartilage and in endochondral ossification. Proc Natl Acad Sci U S A 101: 17192–17197.
30. Ryu JH, Kim SJ, Kim SH, Oh CD, Hwang SG, et al. (2002) Regulation of the chondrocyte phenotype by beta-catenin. Development 129: 5541–5550.
31. Lefebvre V, Li P, de Crombrugghe B (1998) A new long form of Sox5 (L-Sox5), Sox6 and Sox9 are coexpressed in chondrogenesis and cooperatively activate the type II collagen gene. EMBO J 17: 5718–5733.
32. Akiyama H, Chaboissier MC, Martin JF, Schedl A, de Crombrugghe B (2002) The transcription factor Sox9 has essential roles in successive steps of the chondrocyte differentiation pathway and is required for expression of Sox5 and Sox6. Genes Dev 16: 2813–2828.
33. Akiyama H, Lyons JP, Mori-Akiyama Y, Yang X, Zhang R, et al. (2004) Interactions between Sox9 and beta-catenin control chondrocyte differentiation. Genes Dev 18: 1072–1087.
34. Kumar D, Lassar AB (2009) The transcriptional activity of Sox9 in chondrocytes is regulated by RhoA signaling and actin polymerization. Mol Cell Biol 29: 4262–4273.
35. Zhu M, Chen M, Zuscik M, Wu Q, Wang YJ, et al. (2008) Inhibition of beta-catenin signaling in articular chondrocytes results in articular cartilage destruction. Arthritis Rheum 58: 2053–2064.
36. Weng LH, Ko JY, Wang CJ, Sun YC, Wang FS (2012) Dkk-1 promotes angiogenic responses and cartilage matrix proteinase secretion in synovial fibroblasts from osteoarthritic joints. Arthritis Rheum 64: 3267–3277.
37. Ouskova G, Spellerberg B, Prehm P (2004) Hyaluronan release from Streptococcus pyogenes: export by an ABC transporter. Glycobiology 14: 931–938.
38. Hamerman D, Sasse J, Klagsbrun M (1986) A cartilage-derived growth factor enhances hyaluronate synthesis and diminishes sulfated glycosaminoglycan synthesis in chondrocytes. J Cell Physiol 127: 317–322.
39. Prehm P, Schumacher U (2004) Inhibition of hyaluronan export from human fibroblasts by inhibitors of multidrug resistance transporters. Biochem Pharmacol 68: 1401–1410.
40. Prehm P (2005) Inhibitors of hyaluronan export prevent proteoglycan loss from osteoarthritic cartilage. J Rheumatol 32: 690–696.
41. Strazielle N, Ghersi-Egea JF (2013) Physiology of blood-brain interfaces in relation to brain disposition of small compounds and macromolecules. Molecular pharmaceutics 10: 1473–1491.
42. Correa S, Binato R, Du Rocher B, Castelo-Branco MT, Pizzatti L, et al. (2012) Wnt/beta-catenin pathway regulates ABCB1 transcription in chronic myeloid leukemia. BMC cancer 12: 303.

SCIENTIFIC REPORTS

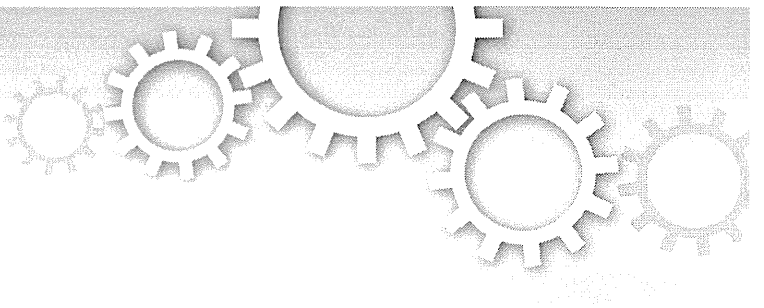

OPEN

SUBJECT AREAS:
RNA SPLICING
GENETICS RESEARCH

Received
25 July 2014

Accepted
13 October 2014

Published
30 October 2014

Correspondence and requests for materials should be addressed to K.O. (ohnok@med.nagoya-u.ac.jp)

HnRNP C, YB-1 and hnRNP L coordinately enhance skipping of human *MUSK* exon 10 to generate a Wnt-insensitive MuSK isoform

Farhana Nasrin, Mohammad Alinoor Rahman, Akio Masuda, Kenji Ohe, Jun-ichi Takeda & Kinji Ohno

Division of Neurogenetics, Center for Neurological Diseases and Cancer, Nagoya University Graduate School of Medicine, Nagoya, Aichi, Japan.

Muscle specific receptor tyrosine kinase (MuSK) is an essential postsynaptic transmembrane molecule that mediates clustering of acetylcholine receptors (AChR). *MUSK* exon 10 is alternatively skipped in human, but not in mouse. Skipping of this exon disrupts a cysteine-rich region (Fz-CRD), which is essential for Wnt-mediated AChR clustering. To investigate the underlying mechanisms of alternative splicing, we exploited block-scanning mutagenesis with human minigene and identified a 20-nucleotide block that contained exonic splicing silencers. Using RNA-affinity purification, mass spectrometry, and Western blotting, we identified that hnRNP C, YB-1 and hnRNP L are bound to *MUSK* exon 10. siRNA-mediated knockdown and cDNA overexpression confirmed the additive, as well as the independent, splicing suppressing effects of hnRNP C, YB-1 and hnRNP L. Antibody-mediated *in vitro* protein depletion and scanning mutagenesis additionally revealed that binding of hnRNP C to RNA subsequently promotes binding of YB-1 and hnRNP L to the immediate downstream sites and enhances exon skipping. Simultaneous tethering of two splicing *trans*-factors to the target confirmed the cooperative effect of YB-1 and hnRNP L on hnRNP C-mediated exon skipping. Search for a similar motif in the human genome revealed nine alternative exons that were individually or coordinately regulated by hnRNP C and YB-1.

Neuromuscular junction (NMJ) is the site of communication between motor neurons and muscle fibers for neuromuscular signal transmission to ensure proper muscle contraction. A series of complex signaling cascades are involved in the formation of the neuromuscular synapse. Prior to the arrival of nerve terminals at muscle fibers, aneural acetylcholine receptor (AChR) clusters form in the central region of muscle fibers[1–4], a phenomenon termed prepatterning. Subsequently, motor axons are guided to prospective prepatterned synaptic regions, and upon its arrival agrin is released from the nerve terminal[5,6]. Agrin interacts with LRP4 (low-density lipoprotein receptor-related protein 4) and stimulates the association between LRP4 and MuSK (muscle specific receptor tyrosine kinase) to activate MuSK[7–9]. Activation of MuSK induces AChR clustering. AChR clusters are thus highly concentrated in the postsynaptic membrane, where the NMJ forms.

MuSK harbors specific domains to respond to agrin and Wnt ligands. The ectodomain of MuSK has three immunoglobulin (Ig)-like domains (Ig1, Ig2, and Ig3) and a frizzled-like cysteine-rich domain (Fz-CRD)[10–12] (Fig. 1). Frizzled proteins, receptors for Wnt-ligands, have ten highly conserved cysteine residues forming five disulfide bonds, which are essential for forming a compact folding structure[13] (Fig. S1). MuSK Fz-CRD also has ten conserved cysteine residues observed in Frizzled proteins. Crystal structure of MuSK Fz-CRD indeed revealed a five-disulfide-bridged domain structure[12]. Human Fz-CRD is encoded by exon 10 coding for 6 cysteines and exon 11 coding for 4 cysteines[14,15]. In human, *MUSK* generates six splice variants according to ENSEMBL 76, although two are short variants with unknown functional significance. In two of the four remaining splice variants in human, exon 10 encoding 6 out of 10 essential cysteines in Fz-CRD is alternatively skipped (Isoforms C and D, Fig. S2c). In contrast to human, however, mouse *Musk* exon 10 is constitutively expressed according to the annotations by RefSeq, ENSEMBL 76, and GENCODE M2.

The first Ig-like domain (Ig1) of MuSK is required for agrin to stimulate MuSK phosphorylation via LRP4[9]. Phosphorylation and activation of MuSK can also be promoted by Wnt proteins by interacting with Fz-CRD. In mouse C2C12 myotubes, Wnt9a and Wnt11 can stimulate MuSK phosphorylation by interacting with Fz-CRD

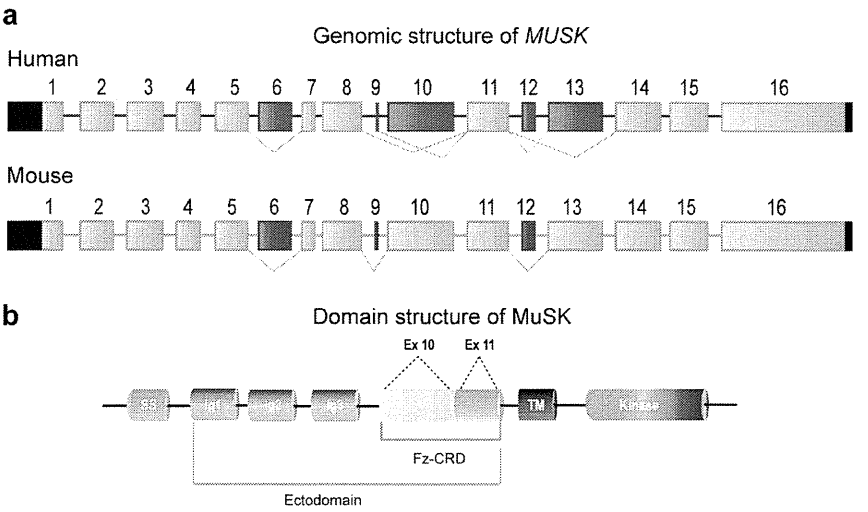

Figure 1 | Structures of human and mouse MuSK. (a) Genomic structures of human *MUSK* and mouse *Musk* genes. Constitutive and alternative exons are shown in green and red boxes, respectively. Black boxes indicate untranslated regions (UTRs) and thin lines indicate introns. Alternative skipping of exons annotated in ENSEMBL 76 are shown by blue connecting lines. (b) Domain structure of MuSK. Fz-CRD is a Wnt-responsive domain encoded by exon 10 coding for 6 cysteines (light blue-colored region of Fz-CRD) and exon 11 coding for 4 cysteines (yellow-colored region of Fz-CRD) in human. SS, signal sequence; TM, transmembrane domain.

and induce AChR clustering, which requires LRP4, but not agrin[16]. In another study, Wnt4 has been shown to induce MuSK phosphorylation by interacting with Fz-CRD in COS7 and HEK293T cells and Wnt4 facilitates mouse NMJ formation *in vivo*[17]. Muscle prepatterning in zebrafish is also facilitated by interaction of Wnt11r with Fz-CRD of a MuSK homolog, *unplugged*[18], which is mediated by enhancing endocytosis of MuSK[19]. In zebrafish, *unplugged*/MuSK has three splice variants: SV1 lacks Ig-like domains 1 to 3 but retains Fz-CRD, and is not responsive to agrin; SV2 lacks Fz-CRD and is not responsive to Wnt; and the full-length isoform that can respond to both agrin and Wnt[18]. Subsequent studies revealed that agrin-non-responsive SV1 is expressed in embryos, which is substituted for by the full-length isoform in adults[18,20,21]. MuSK Fz-CRD additionally plays an important role in motor nerve axon guidance in pathfinding in zebrafish[20,21]. Partial deletions of Fz-CRD have been analyzed in quail QT-6 fibroblasts[22]. Artificial deletion of 6 Fz-CRD cysteines or 4 Fz-CRD cysteines caused lack of an activity for MuSK-rapsyn co-clustering[22]. Amino acids 760 to 820 in the cytoplasmic domain of MuSK, however, have later been shown to be sufficient to confer interaction with rapsyn[23]. As Fz-CRD is an important and obligatory domain of MuSK for Wnt-mediated AChR clustering in zebrafish[18–21] and mouse C2C12 myotubes[16,17], the two discordant reports in zebrafish[22,23] may indicate that Fz-CRD has an additional enhancing effect on MuSK-rapsyn interaction or plays another role in Wnt-mediated AChR clustering. Considering the functional significance of 10 cysteines in Fz-CRD, we humans are likely to have acquired an evolutionally novel Wnt-insensitive MuSK isoform lacking 6 essential cysteines, but the underlying mechanisms of alternative skipping of *MUSK* exon 10 remain unknown.

HnRNP C is a nuclear RNA-binding protein that associates with nascent mRNA transcripts, which plays roles in pre-mRNA splicing[24], mRNA stability[25], and translational modulation[26]. HnRNP C has recently been identified as a molecular ruler to classify RNA polymerase II transcripts for export into two categories: a long mRNA and a short uridine-rich small nuclear RNA (U snRNA)[27]. The Y box-binding protein (YB-1) is a member of the cold shock domain (CSD) protein family, which has binding specificity for both DNA and RNA. YB-1 has multiple roles including transcriptional regulation, translational control, DNA repair, and pre-mRNA splicing[28,29]. HnRNP L is another nuclear RNA-binding protein and a global splicing regulator[30–38]. It also functions in polyadenylation and mRNA stability[39,40].

In the present study, we have dissected the underlying mechanisms of alternative splicing of human *MUSK* exon 10. We first characterized splicing regulatory *cis*-elements by scanning mutagenesis. We then identified that the alternative skipping of *MUSK* exon 10 is coordinately modulated by binding of three splicing suppressors (hnRNP C, YB-1, and hnRNP L) to an exonic splicing silencer (ESS) that is unique to human *MUSK* exon 10. Remarkably, hnRNP C is the master regulator in this regulatory process, and YB-1 and hnRNP L have additive effects to efficiently achieve splicing suppression.

Results

Alternative splicing of *MUSK* exon 10 is unique to human. Since exons 9 (7 nucleotides) and 10 (264 nucleotides) of human *MUSK* are alternatively spliced according to the gene annotation databases, we initially examined the differential selection of these two exons in human skeletal muscle. Using total RNA isolated from human skeletal muscle (Clontech), fragments spanning exons 8 to 11 were amplified by RT-PCR (Fig. S2d). Sequencing of the RT-PCR products revealed three splicing isoforms: (i) exons 9 and 10 included; (ii) exon 10 skipped; and (iii) exons 9 and 10 skipped (Fig. S2f). We could not detect any transcript that skipped only exon 9. We also performed a similar experiment using total RNA isolated from immortalized human myogenic KD3 cells and primary human myoblasts (SkMC), and obtained similar results (Fig. S2d and f). The three observed splicing isoforms are not correctly mapped to the human genome in UCSC Genes, RefSeq, ENCODE/GENCODE Ver. 19 and H-Inv ver. 8.3. As cDNA sequences registered in these annotation databases are correct, a short exon 9 that is comprised of only 7 nucleotides is likely to have precluded correct mapping of cDNAs to the human genome. We also confirmed lack of alternative splicing of mouse *Musk* exon 10 in 10 different skeletal muscle tissues as well as in C2C12 mouse myoblasts (Figs. S2e and S7c). Lack of alternative splicing of mouse *Musk* exon 10 is correctly annotated in all of the gene annotation databases shown above. In this study, we investigated the underlying mechanisms of alternative skipping of exon 10 unique to human.

Construction of minigenes for splicing analysis. We first constructed a human *MUSK* minigene in pcDNA3.1D/V5/His-TOPO expression vector (Invitrogen) spanning exons 8 to 11 (Fig. 2a). Exon 10 in the pcDNA3.1 minigene was alternatively spliced in HeLa cells,

as we observed in human skeletal muscle. We next inserted exon 10 and flanking intronic sequences (245 nucleotides in the upstream intron and 200 nucleotides in the downstream intron) into the modified exon-trapping vector pSPL3[41], which carried two proprietary constitutive exons on each end (Fig. S3a). The pSPL3-human-*MUSK* minigene (H-iE10i) successfully recapitulated alternative splicing of exon 10 in HeLa cells (Fig. S3a). Serial deletions of intronic nucleotides from both ends of H-iE10i revealed that the shortest minigene (H-iE10i-Δ6) that carried 100 nucleotides in the upstream intron and 60 nucleotides in the downstream intron was still alternatively spliced like H-iE10i in HeLa cells (Fig. S3a). This minigene was termed pSPL3-human-*MUSK* (pH-wt) (Fig. 2b) and used in the subsequent experiments.

We also constructed a similar minigene harboring mouse exon 10 and flanking intronic sequences, pSPL3-mouse-MuSK (pm-wt), and found that exon 10 is constitutively included in this minigene in HeLa cells (Fig. 2b). As the mouse minigene was not alternatively spliced even in human cells, we assumed that nucleotides unique to human enabled alternative splicing of exon 10. We confirmed that our minigene was similarly alternatively spliced in KD3 cells and HeLa cells (Fig. 2a and b). Due to better transfection efficiency, we used HeLa cells and pH-wt/pm-wt in the following studies.

Identification of two exonic splicing silencer (ESS) blocks in human exon 10. We next searched for exonic/intronic segments carrying splicing *cis*-elements in pH-wt. To this end, we constructed chimeric minigenes made of variable combinations of human and mouse segments (Fig. 2c). We found that the introduction of mouse exon 10 into pH-wt resulted in constitutive splicing (pH-EC in Fig. 2c). We next introduced the first or second

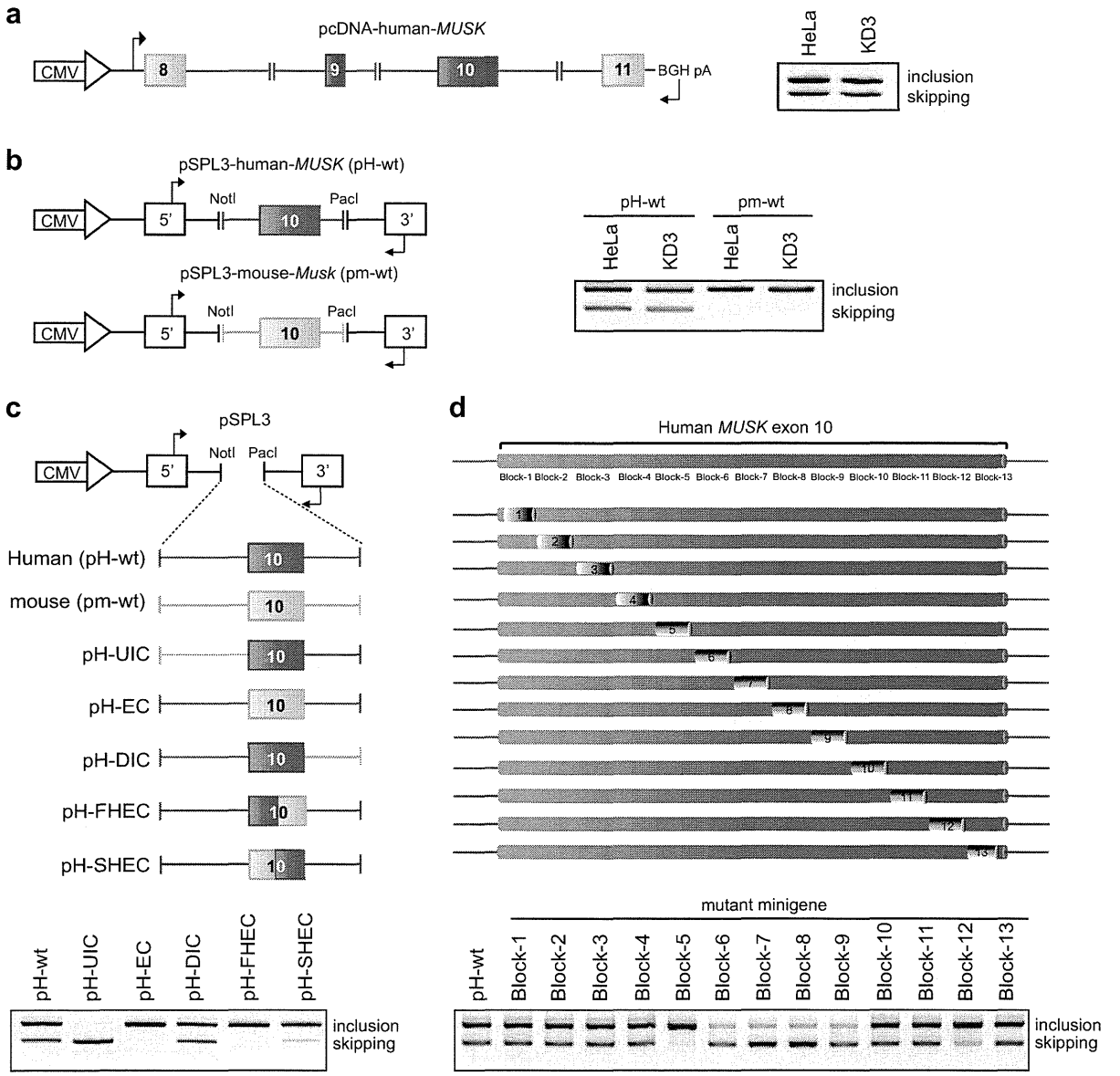

Figure 2 | Construction of minigenes and systematic identification of splicing regulatory *cis*-elements. (a) Structure of human *MUSK* minigene in pcDNA3.1D vector (pcDNA-human-*MUSK*). RT-PCR of this minigene in HeLa and KD3 cells are shown at right. Alternatively and constitutively spliced regions are shown in red and green, respectively. (b) Structure of pSPL3 minigene harboring *MUSK/Musk* exon 10 and flanking introns originated from human (pSPL3-human-*MUSK*, termed pH-wt) and mouse (pSPL3-mouse-*Musk*, termed pm-wt). RT-PCR of these minigenes in HeLa and KD3 cells are shown at right. (c) Schematic of chimeric constructs of pSPL3-human-*MUSK* minigene partially replaced by corresponding mouse sequences shown in green. RT-PCR of each chimeric minigene in HeLa cells is shown below. (d) Schematic of *cis*-regulatory block-scanning mutagenesis of *MUSK* exon 10 in the context of pSPL3-human-*MUSK* (pH-wt) minigene. A 20-nucleotide heterologous sequence of 5′-TCAGTATGACTCTCAGTATG-3′ is introduced into each block. RT-PCR of pH-wt and 13 block-mutant minigenes in HeLa cells are shown bellow. Arrows point to primer positions in (a), (b), and (c).

half of mouse exon 10 into pH-wt, and found that both constructs resulted in constitutive splicing (pH-FHEC and pH-SHEC in Fig. 2c). To specifically identify exonic splicing *cis*-elements, we sequentially introduced a 20-nucleotide heterologous sequence block (5′-TCAGTATGACTCTCAGTATG-3′), which was previously reported to have no effect on splicing[37,42] (Fig. 2d). We scanned the entire exon 10 by substituting 13 blocks excluding the first and last three nucleotides of the exon. The block scanning mutagenesis detected a potential ESS in two separate blocks (blocks 5 and 12) and a potential exonic splicing enhancer (ESE) in four consecutive blocks (blocks 6, 7, 8, and 9) (Fig. 2d). As skipping of exon 10 has a prospective inhibitory effect on AChR clustering, we dissected the mechanisms associated with ESSs in this communication.

Dissection of ESS blocks on a nucleotide level and detection of *trans*-acting factors. We next dissected the identified ESS blocks on a nucleotide level. Alignment of human and mouse blocks 5 (ESS5) and 12 (ESS12) revealed three and two discordant nucleotides, respectively. Artificial introduction of discordant nucleotides into ESS5 (pH-mB5) and ESS12 (pH-mB12) resulted in profound and moderate loss of exon skipping, respectively (Fig. 3a and b), which were consistent with the block-scanning mutagenesis experiments (Fig. 2d). Therefore, the splicing suppressive effect of ESS5 was stronger than that of ESS12.

The vast majority of splicing enhancer and silencer sequences have been reported to function through the binding of cognate regulatory proteins[43]. To determine if potential *trans*-acting factors stably interact with the ESS sequences, binding reactions were performed with a HeLa nuclear extract and an RNA probe harboring human or mouse ESS5 sequence (Fig. 3c). An RNA mobility shift assay with a native gel showed three slow migrating complexes with the ^{32}P-labeled human ESS5 RNA probe (H-B5) (Fig. 3d). In contrast, the two slow migrating complexes observed with H-B5 were not visible with the mouse ESS5 RNA probe (m-B5). We also performed a similar experiment with human/mouse ESS12 RNA probes, but could not detect any differentially associated complex (Fig. S3b and c). We thus focused on identification of the proteins bound to ESS5.

HnRNP C, YB-1, and hnRNP L are bound to human ESS5. We next performed an RNA affinity purification assay using a HeLa nuclear extract and a biotinylated ESS5 RNA probe (Fig. 3c). Three distinct bands of ~70, ~50, and ~40 kD were associated with the wild-type human ESS5 RNA probe (H-B5) but not with the mouse probe (m-B5) or a partially deleted human probe (H-B5Δ5) (Fig. 3e). Mass spectrometry analysis of the excised bands disclosed that the identified bands were hnRNP L, YB-1, and hnRNP C, respectively, which were confirmed by immunoblotting using respective antibodies [anti-hnRNP L 4D11 (sc-32317, Santa Cruz Biotechnology), anti-YB1 (A303-230A, Bethyl Laboratories), and anti-hnRNP C1/C2 4F4 (SC-32308, Santa Cruz Biotechnology)] (Fig. 3f). Similar analysis with ESS12 detected no differentially associated molecule (Fig. S3d).

HnRNP C, YB-1, and hnRNP L coordinately enhance skipping of human *MUSK* exon 10. We next examined the effects of the identified *trans*-factors on skipping of exon 10 by siRNA-mediated downregulation of the individual factors in HeLa cells. We first confirmed efficient downregulation of each factor (Fig. 4a). Downregulation of hnRNP C resulted in a significant loss of exon skipping (Fig. 4b). Similarly, downregulation of YB-1 and hnRNP L caused a loss of exon skipping, but to a lesser extent compared to hnRNP C. Downregulation of all three *trans*-factors exerted a more prominent effect than hnRNP C alone. Thus, YB-1 and hnRNP L are likely to have additive effects on exon skipping. We observed similar alterations in alternative splicing patterns with a second set of siRNAs targeting different sites of each mRNA (Fig. S3e).

We next overexpressed cDNA of each *trans*-factor in HeLa cells. We first confirmed the expression of each cDNA by immunoblotting (Fig. 4c). As expected, overexpression of hnRNP C induced skipping of exon 10 (Fig. 4d). A similar increase in exon skipping was also observed with overexpression of YB-1 and hnRNP L, but to a lesser extent compared to hnRNP C. The most prominent skipping was observed when all three factors were overexpressed together, which was consistent with the knockdown results.

HnRNP C is a critical regulator in inducing exon skipping, whereas YB-1 and hnRNP L have augmenting effects. Having identified the critical *cis*-element and their cognate-binding partners, we next analyzed the molecular basis of specific binding of each *trans*-factor to ESS5. HnRNP C prefers to bind to poly-T stretch motifs[24,44] and both hnRNP L and YB-1 prefer to bind to C/A-rich motifs[29,32,45]. ESS5 carries a stretch of five T's in the first half of the block and a C/A-rich sequence in the second half of the block (H-B5 in Fig. 5a and b). *In vitro* SELEX studies of hnRNP L demonstrated that CACA and ACAC sequences confer high-affinity binding motifs and that CAAC and CACC confer low-affinity binding motifs for hnRNP L[32], where motifs present in ESS5 are underlined. On the contrary, *in vitro* SELEX studies of YB-1 revealed that CATC and CACC sequences confer high-affinity binding motifs for YB-1[29], where a motif present in ESS5 is underlined. Therefore, the second half of ESS5 harbors overlapping binding motifs of both YB-1 and hnRNP L. To characterize the precise binding sites of the associated factors, we introduced a series of artificial point mutations into the human ESS5 RNA probe and checked the binding of each factor by RNA-affinity purification followed by Western blotting (Fig. 5a and b). We observed that poly-T stretch-disrupting mutations in the first half indeed abolished the binding of hnRNP C (Fig. 5a, lanes 3, 4, and 5), and four or more consecutive T-nucleotides are necessary for hnRNP C binding. To our surprise, we noticed that binding of YB-1 and hnRNP L was also compromised along with disruption of the hnRNP C binding (Fig. 5a, lanes 3, 4 and 5). This suggested that binding of YB-1 and hnRNP L was dependent on poly T-stretch. On the other hand, introduction of mutations in the second half (C/A-rich sequences) compromised binding of YB-1 and hnRNP L, but not of hnRNP C (Fig. 5b). In addition, characterization of essential nucleotides for binding of hnRNP L (CAACA) and YB-1 (ACACCT) revealed that binding motifs of hnRNP L and YB-1 indeed overlap (CAACACCT) in the second half of ESS5, where the overlapping nucleotides are underlined. Considering the overall findings (Fig. 5c), we predicted that binding of hnRNP C to the poly-T stretch facilitates the binding of YB-1 and hnRNP L to the adjacent downstream site. To test this hypothesis, we depleted hnRNP C from a HeLa nuclear extract using a specific antibody (Fig. S4a) and performed RNA affinity purification assays. As we had expected, depletion of hnRNP C nullified the binding of YB-1 and hnRNP L (Fig. S4b).

Binding of hnRNP C, YB-1, and hnRNP L to ESS5, but not to the other site, induces skipping of *MUSK* exon 10. Having characterized a coordinated regulation of hnRNP C, YB-1, and hnRNP L on skipping of exon 10, we next examined the additive effect of YB-1 or hnRNP L on hnRNP C-mediated exon skipping. To this end, we made a reporter minigene (pSPL3-human-*MUSK*-MS2-PP7), in which the bacteriophage MS2 coat protein-binding site was substituted for the native 'TTTTTCT' sequence in the first half of ESS5 (the binding site of hnRNP C), and the bacteriophage PP7 coat protein-binding site was substituted for the native 'CAACACCTC' sequence in the second half of ESS5 (the binding site of YB-1 and hnRNP L) (Fig. 5d). We also made cDNA fusion constructs, hnRNP C-MS2, YB-1-PP7, and hnRNP L-PP7, to artificially tether splicing *trans*-factors to the respective sites. As expected, tethering of MS2-tagged hnRNP C alone efficiently induced exon skipping of 79%

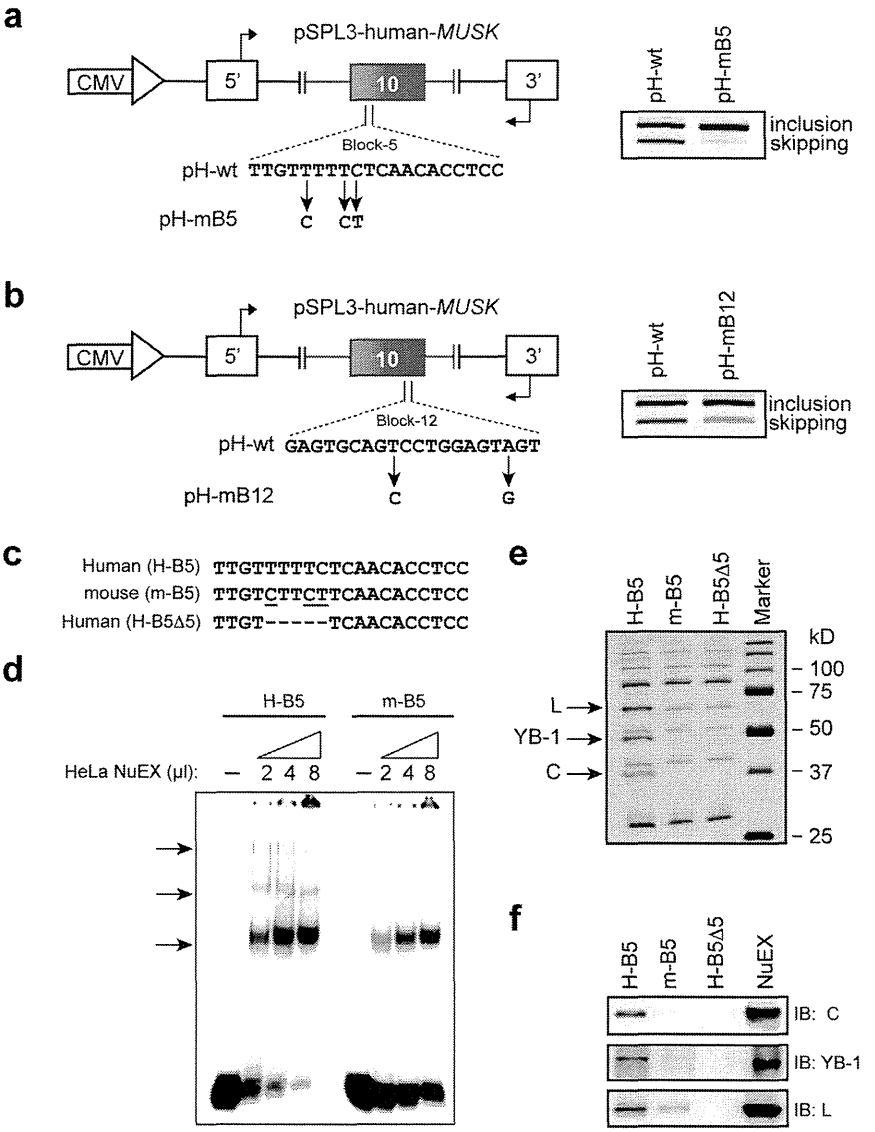

Figure 3 | HnRNP C, YB-1 and hnRNP L bind to exon 10 of human *MUSK*. (a, b) Mouse nucleotides are introduced into ESS5 (a) and ESS12 (b) of pH-wt to generate pH-mB5 and pH-mB12, respectively. RT-PCR of each mutated minigene in HeLa cells is compared with that of pH-wt. Primer positions are shown by arrows. (c) Sequences of ESS5 RNA probes carrying human (H-B5), mouse (m-B5), and partially deleted (H-B5Δ5) sequences. (d) ^{32}P-labeled H-B5 or m-B5 RNA probe was incubated in the presence or absence of HeLa nuclear extract (NuEX) and resolved on a native polyacrylamide gel to observe free and protein-bound RNA species (arrows). (e) Coomassie blue staining of RNA affinity-purified products from HeLa nuclear extract using the indicated biotinylated RNA probes. Three proteins of ~70, ~50, and ~40 kDa (arrows) are differentially associated with H-B5 compare to m-B5 and H-B5Δ5. Mass spectrometry analysis revealed that the three proteins are HnRNP L (L), YB-1, and hnRNP C (C). (f) Immunoblotting (IB) of RNA affinity purified proteins in panel (e) with the indicated antibodies.

(Fig. 5e, lane 3). Tethering of PP7-tagged YB-1 and hnRNP L without tethering MS2-tagged hnRNP C induced exon skipping of 52% (Fig. 5e, lane 5) and 36% (Fig. 5e, lane 8), respectively. In contrast, hnRNP C, YB-1, or hnRNP L without a tethering tag did not induce exon skipping (Fig. 5e, lanes 2, 4 and 7), suggesting that ESS5 was the only site where these factors were able to bind and function. We also confirmed that MS2- or PP7-tagged factor has no effect on a minigene lacking MS2- or PP7-binding site (Fig. S4d). Simultaneous recruitment of hnRNP C with either YB-1 or hnRNP L further induced exon skipping (Fig. 5e, lanes 6 and 9), which reconfirmed the additive effects of YB-1 and hnRNP L on hnRNP C-mediated splicing suppression.

RNA-dependent interaction of hnRNP C, YB-1, and hnRNP L and search for similar targets in other human genes. We next examined the molecular interaction between the three *trans*-factors. Co-immunoprecipitation revealed that HnRNP C and hnRNP L were bound in an RNA-dependent manner (Fig. S5a), whereas hnRNP C and YB-1 were not (Fig. S5b). Similarly, hnRNP L and YB-1 were bound in an RNA-dependent manner (Fig. S5c), which was consistent with a previous report[45].

We further asked if coordinated splicing regulation by hnRNP C, YB-1, hnRNP L is unique to *MUSK* exon 10. As hnRNP L has highly degenerative SELEX motifs, which are overlapping with YB-1 motifs, we analyzed coordinated splicing only by hnRNP C and YB-1. Search for adjacent hnRNP C- and YB-1-binding motifs in human alternative cassette exons and flanking introns detected 378 candidate sites. We randomly selected 37 exons and analyzed alternative splicing in HeLa cells in the presence of siCont, siC, siYB-1, and siC/siYB-1. We found that alternative splicing events of 9 exons were affected by hnRNP C and/or YB-1 in HeLa cells, whereas 13 exons were not expressed and 15 exons were not alternatively spliced or affected

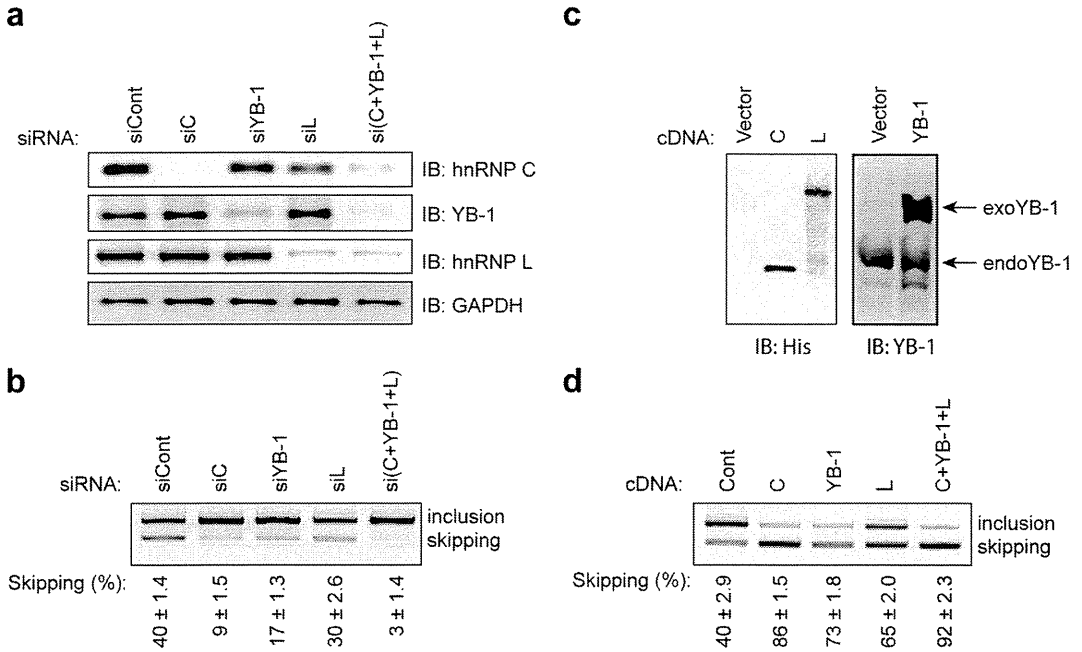

Figure 4 | HnRNP C, YB-1, and hnRNP L coordinately promote skipping of *MUSK* exon 10. (a) Immunoblotting (IB) using the indicated antibodies after gene knockdown with siRNA against control (siCont), hnRNP C (siC), YB-1 (siYB-1), and hnRNP L (siL) in HeLa cells. (b) RT-PCR of pSPL3-human-*MUSK* (pH-wt) minigene in HeLa cells treated with the indicated siRNAs. The mean and SD ($n = 3$) of the ratio of exon skipping in each treatment is shown below the gel image. (c) Immunoblotting (IB) with the indicated antibodies after cDNA overexpression of hnRNP C, YB-1, and hnRNP L in HeLa cells. Endogenous (endo) and exogenous (exon) YB-1 proteins are pointed by arrows. (d) RT-PCR of pH-wt minigene in HeLa cells co-transfected with the indicated cDNAs. The mean and SD ($n = 3$) of the ratio of exon skipping in each treatment is shown below the gel image.

by knockdown (Fig. S6). Among the 9 exons, 3 exons were coordinately skipped by hnRNP C and YB-1 (Fig. S6a).

Expressions of splicing repressing hnRNP C and YB-1 are reduced with muscle differentiation. As MuSK is a muscle-specific receptor protein having an important role in muscle development and function, we next examined the splicing profile of human *MUSK* exon 10 in different stages of myogenic differentiation. We cultured immortalized human myogenic KD3 cells in differentiation medium for four days to make myotubes (Fig. 6a). RT-PCR spanning endogenous *MUSK* exon 10 at different time points revealed that skipping of exon 10 was suppressed on and after differentiation day 3 (Fig. 6b, and Supplementary Table 1). Similarly, myotube differentiation suppressed skipping of *MUSK* exon 10 in primary human myoblasts (SkMC) (Figs. S7a, b, and 6c), and skipping of exon 10 constitutes only 12% in human skeletal muscle (Fig. 6c and Supplementary Table 1). Thus, skipping of exon 10 is a minor event in any differentiation stages of myogenic and muscle cells.

In KD3 cells, we found that the expressions of hnRNP C and YB-1 were indeed decreased on and after day 3, whereas the expression level of hnRNP L was not significantly changed at the mRNA (Fig. 6d) and protein (Fig. 6e) levels. Therefore, reduction of hnRNP C and YB-1 in the course of muscle differentiation causes reduction of skipping of human *MUSK* exon 10 to produce a Wnt-sensitive MuSK isoform.

Discussion

In this study, we have identified splicing regulatory *cis*-elements and cognate *trans*-factors that drive alternative splicing of human *MUSK* exon 10. HnRNP C enhances exon skipping in coordination with YB-1 and hnRNP L by binding to a regulatory exonic splicing silencer, ESS5. Two splicing suppressive *cis*-elements, ESS5 and ESS12, are recognized by block-scanning mutagenesis, although the ESS activity of ESS12 is not as conspicuous as that of ESS5. Most splicing regulatory ESSs and ESEs function through the binding of cognate regulatory proteins[43]. Indeed, ESS5 is recognized by the three splicing *trans*-factors, but no associated molecules are detected for ESS12. In contrast, the splicing suppressive activity of ESS12 is likely to be regulated by a local secondary structure of pre-mRNA. Alternatively, a binding affinity of a splicing *trans*-factor to ESS12 is too low to be detected by the RNA mobility shift assay and the RNA affinity purification assay.

We have characterized the mutual coordination between the three *trans*-factors. HnRNP C binds to a poly-T stretch in the first half of ESS5, whereas binding motifs of hnRNP L and YB-1 are overlapped in the second half of ESS5. In addition, binding of YB-1 and hnRNP L is dependent on hnRNP C. One possible mechanism for this is that overlapping binding motifs between hnRNP L and YB-1 provoke competitive binding of the two factors. A third molecule, hnRNP C, may rearrange RNA conformation to stabilize the binding of either hnRNP L or YB-1. Similar RNA-mediated stabilization of binding of another RNA-binding protein by a specific RNA-binding protein has been reported in other genes. In *CD45*, hnRNP L stabilizes the binding of hnRNP A1 in exon 4, in which binding of hnRNP A1 and the subsequent splicing suppression is dependent on hnRNP L[34]. The authors demonstrate that hnRNP L interacts with hnRNP A1, which is lost by RNase. In *Tpm1*, splicing of exon 3 is coordinately repressed by PTB and Raver 1[46]. Interaction between PTB and Raver 1, which requires the target RNA, results in a conformational change of the tertiary complex to bring the repressor domain of both molecules in close apposition to synergistically promote exon skipping. Therefore RNA-dependent molecular interaction and coordinated splicing suppression is unlikely to be unique to ESS5 and is likely to be functional in many other alterative splicing events.

Binding of YB-1 and hnRNP L to the same target and the subsequent coordinated splicing regulation have been previously reported[45]. The authors report that overexpression and depletion of either YB-1 or hnRNP L is sufficient to repress and derepress splicing, respectively. In their report, YB-1 exerts a stronger effect

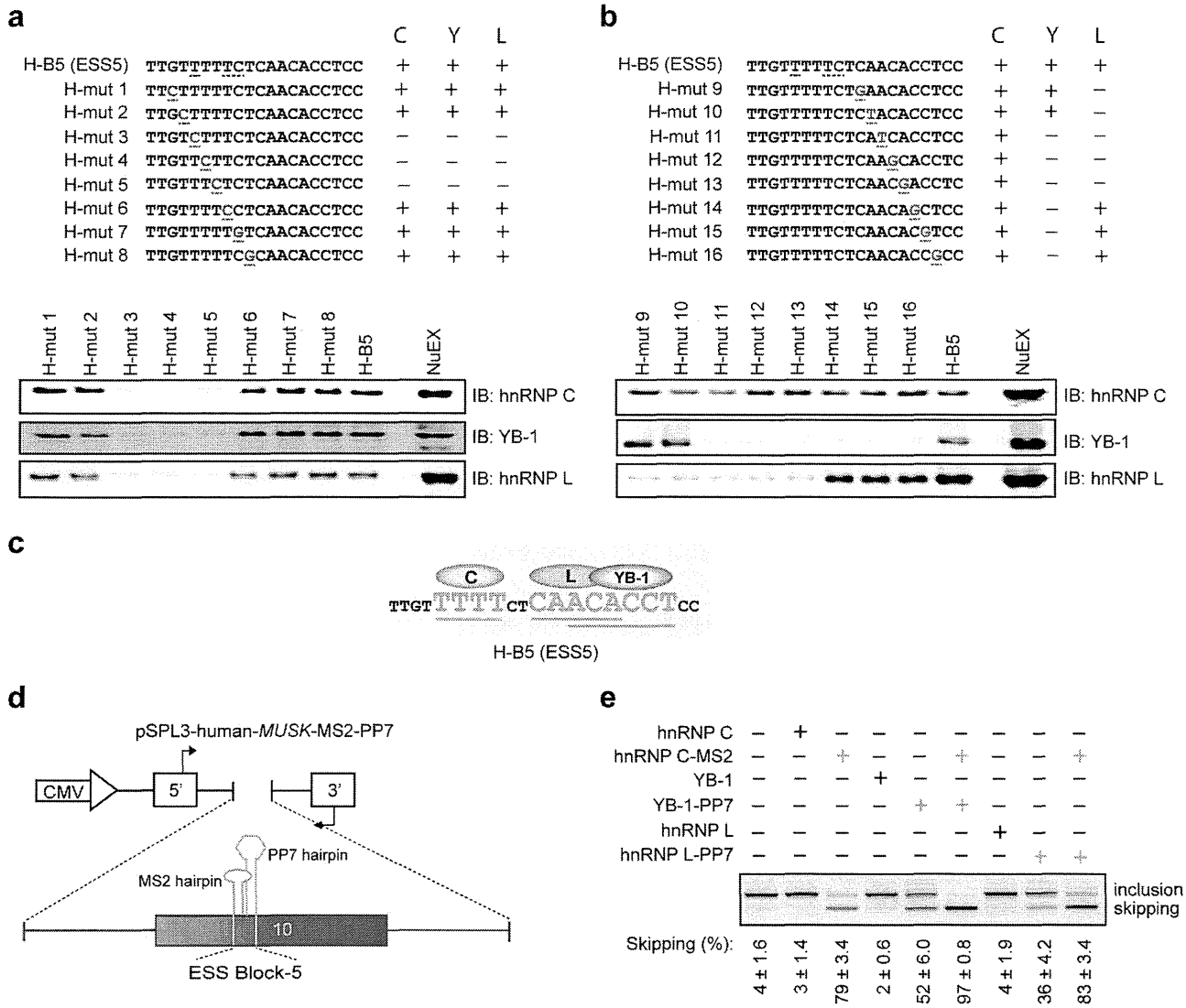

Figure 5 | Binding of hnRNP C, YB-1, and hnRNP L to specific motifs enhances coordinated skipping of *MUSK* exon 10. (a, b) Scanning mutagenesis to map the binding motifs of hnRNP C, YB-1, and hnRNP L in ESS5 (H-B5). RNA probe sequences are shown in the upper panels, where discordant nucleotides between human and mouse are underlined in H-B5 (ESS5). Artificial mutations are shown in red. RNA affinity-purified products are detected by immunoblotting in the lower panels. The results are indicated on the right side by "+" and "−" for positive and negative binding to each probe, respectively. (c) The resulting binding site of each factor from panels (a) and (b) is schematically shown. Essential binding nucleotides are indicated by large green letters and are underlined. (d) Schematic of a reporter minigene (pSPL3-human-*MUSK*-MS2-PP7). MS2 coat protein-binding hairpin RNA (blue) is substituted for the first half of ESS5 (binding site of hnRNP C). Similarly, PP7 coat protein-binding hairpin RNA (orange) is substituted for the second half of ESS5 (binding sites of hnRNP L and YB-1). (e) RT-PCR of pSPL3-human-*MUSK*-MS2-PP7 minigene in HeLa cells that are co-transfected with the indicated effectors. Blue and orange letters match to those in (d). The mean and SD (n = 3) of the ratio of exon skipping in each treatment is shown below the gel image.

than hnRNP L, as in our *MUSK* exon 10. To the best of our knowledge, *MUSK* exon 10 is the first target where coordinated splicing regulation by YB-1 and hnRNP L is dependent on hnRNP C. RT-PCR analysis of 37 targets, where an hnRNP C-binding 'TTTT' motif and a YB-1-binding 'CATC/CACC' motif are adjacent to each other in human alternative cassette exons and flanking introns, revealed three alternative cassette exons that are coordinately skipped by hnRNP C and YB-1. Although detailed functional coordination of hnRNP C and YB-1 on these targets, and involvement of hnRNP L, remain unknown, *MUSK* exon 10 is unlikely to be the only target where hnRNP C, YB-1, and hnRNP L coordinately induce exon skipping.

Recent studies of alternative splicing in different cellular and physiological states have broadened our understanding of the molecular basis for functional selection of a certain isoform in a tissue-specific and developmental stage-specific manner. These studies demonstrated multiple intriguing features of splicing regulatory factor(s) including cell-type specific expression, intracellular localization, post-translational modification on different cellular stimuli, etc. Precise regulation of cellular differentiation is indispensable for the proper development of vertebrate embryo and deregulated differentiation results in diverse human congenital abnormalities including cancers. In human myogenic cells (KD3), skipping of *MUSK* exon 10 is significantly reduced from ~41% to ~22% upon myogenic differentiation, which is in parallel with the reduced expression of hnRNP C and YB-1 (Fig. 6). We also observed a similar expression profile of *MUSK* exon 10 in primary human myoblasts (SkMC) upon myogenic differentiation (Figs. S7a, b and 6c). Reduced expression of hnRNP C, YB-1 and even hnRNP L upon myogenic differentiation is also reported in mouse myoblast cells

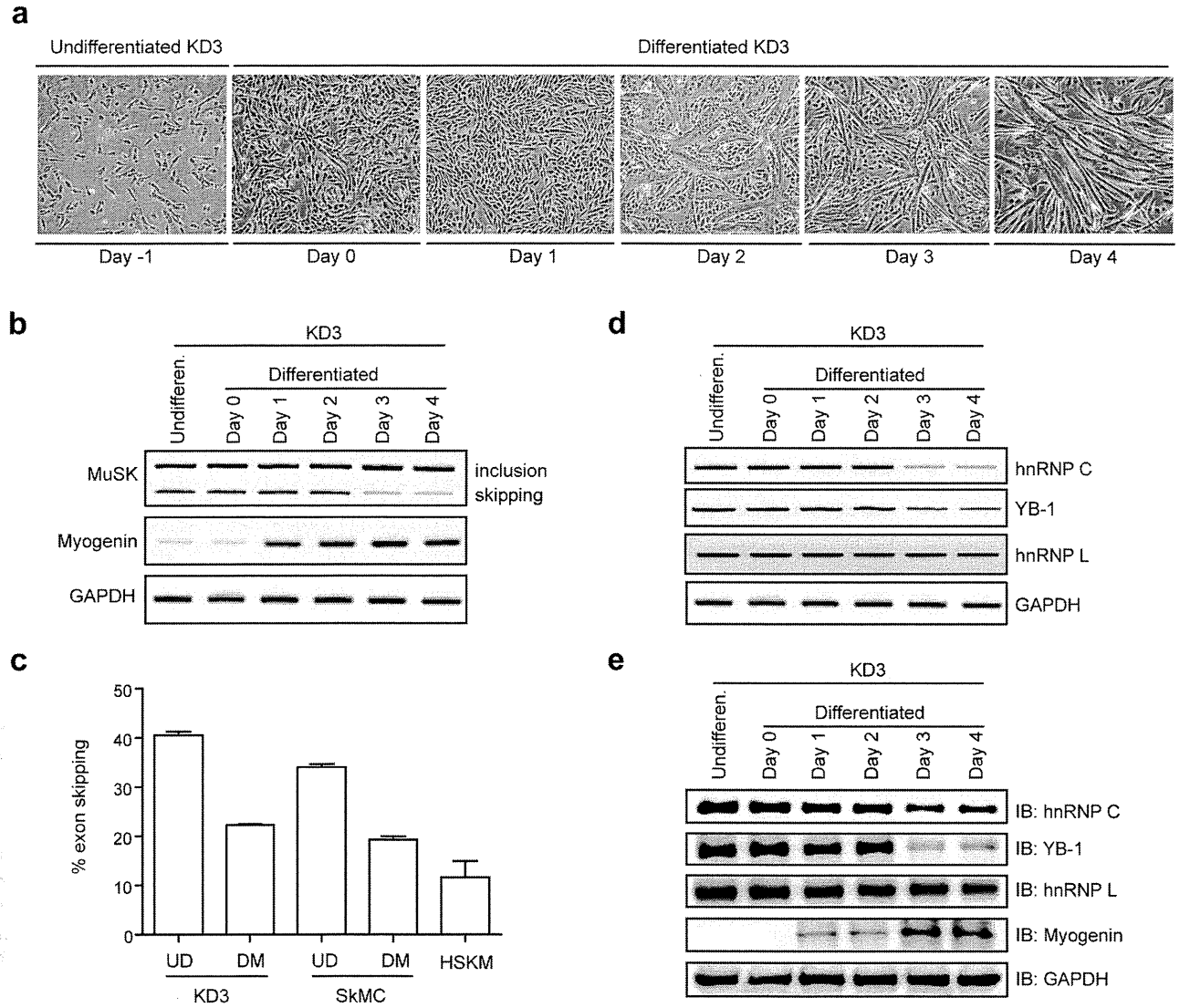

Figure 6 | Suppression of hnRNP C and YB-1 expressions in myogenic differentiation enhances inclusion of *MUSK* exon 10. (a) Phase-contrast images showing a temporal profile of differentiation of KD3 cells. (b) RT-PCR showing alternative splicing of endogenous *MUSK* exon 10 at different differentiation days of KD3 cells. (c) Real-time RT-PCR to quantify endogenous human *MUSK* transcripts. The absolute copy numbers of each isoform (Isoforms A-D, as shown in Fig. S2f) were estimated using total RNA isolated from KD3 cells, primary human myoblasts (SkMC) and human skeletal muscle (HSKM). Then the ratio of exon 10-skipping (including both isoforms C and D as shown in Fig. S2f) was determined (% exon skipping). UD, undifferentiated cells; DM, differentiated myotubes (at day 4 for KD3 and at day 8 for SkMC). Transcripts levels were normalized against GAPDH values. Bars represent mean and SD of three independent experiments. (d, e) Endogenous expression of splicing suppressors by RT-PCR (d) and immunoblotting (e) at different differentiation days of KD3 cells. Expressions of myogenin and GAPDH are shown as internal controls in panels (b), (d), and (e). The same gel image of GAPDH is used in panels (b) and (d).

(C2C12)[47,48]. Therefore, human has evolutionally acquired ESS5 to skip *MUSK* exon 10, whereas downregulation of its *trans*-factors, hnRNP C and YB-1, in muscle differentiation remains unchanged in the course of evolution. It is interesting to note that YB-1 is a negative regulator of C2C12 myoblast differentiation[48]. YB-1 cooperatively interacts with MSX1 that inhibits the expression of MyoD by binding to the core enhancer region (CER) of the MyoD promoter[48]. Therefore, reduction of YB-1 expression in the course of differentiation is physiologically relevant to facilitating myogenic differentiation.

Physiological and evolutional significance of acquisition of an exon 10-skipped Wnt-insensitive MuSK isoform in human remains elusive, although an exon 10-skipped MuSK isoform constitutes a minor fraction in human skeletal muscle. An exon 10-skipped isoform is deficient of Fz-CRD function[16,17]. In *CHRNA1* encoding AChR α subunit, only humans and great apes have acquired alternative inclusion of a non-functional exon P3A, which we have shown to be regulated by hnRNP H[41], PTB[49], and hnRNP L[38]. Although the evolutional significance of having acquired a non-functional exon P3A remains unsolved, skipping of *MUSK* exon 10 is the second defective splicing event that is unique to human. In mammals, *CHRNE* encoding the AChR ε subunit is expressed only at NMJ to promote endplate-specific expression of AChR[50-52]. Similarly, *Colq* encoding collagen Q has two promoters that are activated in slow- and fast-twitch muscles, respectively. In fast-twitch muscles, the Colq-1a promoter is activated only at NMJ[53]. Differentiation-induced inclusion of *MUSK* exon 10, as well as NMJ-specific expression of *CHRNE* and *COLQ*, suggest that human might have acquired NMJ-specific expression of a Wnt-responsive exon 10-included *MUSK* isoform to suppress extra-synaptic formation of AChR clusters. To achieve such beneficial expression, exonic splicing *cis*-elements have evolved to utilize spatiotemporally regulated expressions

of splicing *trans*-factors that were already functional in lower mammals.

Methods

Sources of human skeletal muscle RNA. To scrutinize *MUSK* isoforms in human skeletal muscle, we purchased human skeletal muscle total RNA (Clontech). We also purchased primary human skeletal muscle cells (SkMC, Lonza). Immortalized human myogenic cells (KD3) were kindly provided by Dr. Naohiro Hashimoto (National Center for Geriatrics and Gerontology, Japan)[54–56].

Cell culture and transfection. HeLa and C2C12 cells were cultured in DMEM (Sigma-Aldrich) with 10% fetal bovine serum (FBS, Sigma-Aldrich). SkMC cells were maintained in SkGM medium (Lonza). KD3 cells were grown in high-glucose (4.5 g/ml) DMEM (hDMEM) media containing 20% FCS and 2% Ultroser G serum substitute (PALL). To induce myogenic differentiation in C2C12 or SkMC, the culture medium of confluent cells was switched to DMEM supplemented with 2% horse serum. For myogenic differentiation of KD3 cells, we cultured confluent cells in hDMEM containing 5 μg/ml holo-transferrin (bovine), 10 μg/ml insulin, and 10 nM selenite (TIS, Gibco), as well as 2% FCS. HeLa and KD3 cells were transfected by FuGENE 6 (Roche) and Avalanche (EZT-HSKM-1, EZ Biosystems), respectively.

Construction of *MUSK* minigene for splicing analysis. We constructed human *MUSK* minigene spanning exons 8 to 11 in pcDNA3.1D/ V5-HiS-TOPO vector (Invitrogen) using a proofreading DNA polymerase (PrimeSTAR, Takara). Four PCR products were first amplified: exon 8 to intron 8 (IVS8+389); intron 8 (IVS8-148) to intron 9 (IVS9+121); intron 9 (IVS9-243) to intron 10 (IVS10+202); and intron 10 (IVS10-77) to exon 11. The PCR primers carried additional 5′ sequences that matched to the neighboring amplicons. Amplicons 1/2 and 3/4 were first ligated each other, respectively, and the generated fragments 1/2 and 3/4 were ligated to generate a single fragment to be cloned into pcDNA3.1D/ V5-HiS-TOPO vector. The final product, pcDNA-human-*MUSK*, thus lacked 13865, 5248, and 7426 nucleotides in the middle of introns 8, 9, and 10, respectively.

We also inserted *MUSK/Musk* exon 10 and flanking intronic sequences (245 nucleotides of intron 9 and 200 nucleotides of intron 10) of both human and mouse in the modified exon-trapping vector, pSPL3[41]. The PCR product carried NotI and PacI sites on each for cloning into pSPL3. Artificial mutations and block replacement were engineered into the pSPL3 minigenes using the QuikChange site-directed mutagenesis kit (Stratagene) (Supplementary Table 2).

We made chimeric constructs of pSPL3-human-*MUSK* carrying human and mouse segments using the megaprimer method[57]. At first, we PCR-amplified the desired mouse segment with primers that carried 20 to 25 complementary nucleotides to pSPL3-human-*MUSK* at the 5′ ends. The PCR amplicon was used as a megaprimer for the QuikChange site-directed mutagenesis kit to make chimeric pSPL3-human-*MUSK* minigenes. The entire inserts were sequenced for all the generated clones to ensure absence of PCR artifacts.

RT-PCR and real-time RT-PCR. Total RNA was extracted 40 h after transfection using Trizol (Invitrogen), followed by DNase I treatment (Qiagen). cDNA was synthesized with an oligo-dT primer (Invitrogen) using ReverTra Ace reverse transcriptase (Toyobo). RT-PCR was performed using GoTaq (Promega) (Supplementary Table 3).

Real-time RT-PCR was performed using LightCycler 480 II (Roche) and the SYBR Premix Ex Taq II (Takara) to quantify endogenous human *MUSK* transcripts. The absolute copy numbers of each of *MUSK* isoforms were estimated using specific primers (Supplementary Table 3) and cDNA fragments cloned into pGEM-T as references.

RNA-electrophoretic mobility shift assays (RNA-EMSA). ^{32}P-labeled RNA probes comprised of 20 nucleotides were transcribed *in vitro* with the T7 RiboMAX large-scale RNA production system (Promega) using ^{32}P-UTP as previously reported[58]. The template DNA for transcription was generated by overlap extension PCR using two overlapping primers (Supplementary Table 4), where T7 promoter sequence was introduced at the 5′ end of the forward primer. Binding reactions were carried out using HeLa nuclear extract (CilBiotech) and radiolabeled RNA probes at 30°C for 15 min in a 15-μl reaction mixture, with a final concentration of 3.0 mM $MgCl_2$, 50 mM KCl, 20 mM Tris-HCl (pH 7.5), 0.1 mM EDTA, 0.1% (v/v) Triton X-100, 10% (v/v) glycerol, 3 μg of BSA, 1 μg of tRNA, 4 U RNasin (Promega). RNA-protein complexes were analyzed by 5% polyacrylamide gel electrophoresis (PAGE) at 4°C using 0.5× Tris-borate-EDTA (TBE) buffer. Dried gels were subjected to autoradiography.

RNA affinity purification assay. We synthesized 20-nucleotide biotinylated RNA probes with the T7 RiboMAX large-scale RNA production system (Promega) using 3.0 mM Biotin-14-CTP (Invitrogen) as described previously[38]. The template DNA was generated as described for RNA-EMSA.

The RNA affinity purification method was modified from the previously adopted protocol[38]. Biotinylated RNAs (0.75 nmol) and HeLa nuclear extract (30 μl) (CilBiotech) were mixed in a 500-μl binding buffer [20 mM HEPES, pH 7.8, 150 mM KCl, 0.1 mM EDTA, 1 mM DTT, 1 mM PMSF, 0.05% Triton X, 1× Protease Inhibitor Cocktail (Active Motif)], and were incubated at 30°C for 3 h with gentle agitation. In parallel, 50 μl streptavidin-conjugated beads (Streptavidin-sepharose, GE Healthcare) were blocked with a 1 : 1 mixture of 1 ml binding buffer containing yeast tRNA (0.1 mg/ 100 μl of beads) and 1 ml PBS containing 4% BSA at 4°C with rotation for 1 h. The beads were mixed with the binding solution for 2 h at 4°C with gentle rotation. After washing the beads four times with 1 ml binding buffer, RNA-bound proteins were eluted in SDS loading buffer by boiling at 95°C for 5 min. The isolated proteins were fractionated on a 10% SDS-polyacrylamide gel and stained with Coomassie blue or by immunoblotting.

Mass spectrometry. Mass spectrometry was performed as previously described[38].

Depletion of hnRNP C from nuclear extract. Antibody-mediated depletion of hnRNP C from HeLa cell nuclear extract was performed using Protein G HP spin trap (GE Healthcare) according to the manufacturer's instructions.

siRNA knockdown and minigene splicing. We synthesized the following human siRNAs (Sigma Genosys):

5′-CAACGGGACUAUUAUGAUATT-3′ for hnRNP C;
5′-CCACGCAAUUACCAGCAAATT-3′ for YB-1; and
5′-GAAUGGAGUUCAGGCGAUGTT-3′ for hnRNP L.

We also synthesized a second set of human siRNAs:

5′-GUAGAGAUGAAGAAUGAUATT-3′ for hnRNP C,
5′-AGAAGGUCAUCGCAACGAATT -3′ for YB-1, and
5′-CUACGAUGACCCGCACAAATT-3′ for hnRNP L.

The control siRNA was AllStar Negative Control siRNA (1027281) by Qiagen. Cells were plated 24 h before transfection in six-well culture plates (1.5×10^5 cells/ well). The transfection reagent included each siRNA duplex at a final concentration of 30 nM, 1 μl Lipofectamine 2000 (Invitrogen), and 500 ng minigene in 100 μl Opti-MEM medium. The cells were harvested three days after transfection for RT-PCR and immunoblotting analyses.

cDNA overexpression and minigene splicing. Human hnRNP C cDNA was amplified with total RNA of human skeletal muscle (Clontech), and cloned into pCDNA3.1D/V5-His TOPO (Invitrogen) to make pcDNA-hnRNP C. We previously constructed pcDNA-hnRNP L[38]. The human YB-1 expression vector (pCMV-YB-1-myc-nuc) was kindly provided by Dr. Akira Yokomizo (Kyushu University, Japan)[59]. Cells were plated 24 h prior to transfection in a six-well culture plate (1.5×10^5 cells/ well) and transfected with 1 μg of expression construct(s), 500 ng of the minigene, and 6.0 μl of FuGENE 6 (Roche) in 100 μl Opti-MEM medium. The cells were harvested three days after transfection for RT-PCR and immunoblotting analyses.

Harvesting cells for immunoblotting. Cells were washed twice in PBS and harvested in PBS with 1× Protease Inhibitor Cocktail. After centrifugation at 2,000 × *g* for 5 min, the pellets were resuspended in buffer A [10 mM HEPES-NaOH (pH 7.8), 10 mM KCl, 0.1 mM EDTA, 1 mM DTT, 0.5 mM PMSF, 0.1% Nonidet P-40, 1× Protease Inhibitor Cocktail] and kept for 30 min on ice. After sonication, samples were centrifuged at 20,000 × *g* for 5 min to remove cell debris. The total cell lysate was subjected to immunoblotting.

Tethered function assay. Tethered function assay was performed by co-transfection of a reporter minigene carrying MS2- and PP7-binding sites and effector construct(s) fused to either MS2 or PP7 coat protein. To make pcDNA-hnRNP C-MS2, an insert encoding MS2 was isolated from pcDNA-hnRNP L-MS2[38] using XhoI and XbaI restriction enzymes, purified, and cloned into the respective sites of pcDNA-hnRNP C. We purchased a vector harboring PP7 cDNA (pET22HT-PP7delFG) from Addgene. Using this vector, a PCR product spanning PP7 cDNA was amplified with primers having XhoI and XbaI sites at the 5′ ends. This was subsequently cloned into XhoI/XbaI sites of pcDNA-hnRNP L[38] to obtain pcDNA-hnRNP L-PP7. Using the In-Fusion cloning kit (Clontech), we introduced PP7 cDNA into pCMV-YB-1-myc-nuc to produce pCMV-YB-1-PP7-myc-nuc. The absence of artifacts was confirmed by sequencing the entire inserts. We previously made pcDNA-MS2 harboring only MS2 cDNA[38]. We also cloned only PP7 cDNA into pcDNA3.1D/ V5-HiS-TOPO to make pcDNA-PP7.

To construct a reporter minigene, we substituted the bacteriophage MS2 coat protein-binding hairpin RNA sequence (5′-ACATGAGGATCACCCATGT-3′)[38] for the first half of the ESS5 sequence (5′-TTTTTCT-3′) and PP7 coat protein-binding hairpin RNA sequence (5′-GGCACAGAAGATATGGCTTCGTGCC-3′)[60] for the second half of ESS5 sequence (5′-CAACACCTC-3′) in *MUSK* exon 10 in pSPL3 minigene using the QuikChange site-directed mutagenesis kit.

Antibodies. Antibodies used in this study were anti-hnRNP C1/C2 4F4 (SC-32308, Santa Cruz Biotechnology), anti-YB1 (A303-230A, Bethyl Laboratories), anti-hnRNP L 4D11 (sc-32317, Santa Cruz Biotechnology), anti-His-tag (D291-3, Medical & Biological Laboratories), anti-GAPDH (G9545, Sigma-Aldrich), anti-β-actin C4 (sc-47778, Santa Cruz Biotechnology), anti-myogenin (M-225) (sc-576, Santa Cruz Biotechnology), and anti-U2AF65 MC3 (sc-53942, Santa Cruz Biotechnology).

Co-immunoprecipitation. Protein-protein interactions were studied by the co-immunoprecipitation (Co-IP) experiment using the Nuclear Complex Co-IP kit (Active Motif) according to the manufacturer's instructions, in the presence or absence of RNase (RNase cocktail enzyme mix, Ambion). We incubated 100 μg of HeLa nuclear extract with 2 μg of anti-hnRNP C or anti-YB-1 antibody. We included isotype-matched normal IgG as a control. The binding buffer contained 150 mM

NaCl. The protein G beads with bound molecules were boiled and run on a polyacrylamide gel followed by immunoblotting.

***In silico* search for binding sites of hnRNP C and YB-1 at alternative cassette exons in the human genome.** We first searched for the hnRNP C motif ('TTTT') in human alternative cassette exons and flanking introns according to ENSEMBL 76. We then searched for the YB-1 SELEX motifs (CATC and CACC) within 5 to 16 nucleotides upstream and downstream of the hnRNP C site. We similarly identified hnRNP C-binding sites in iCLIP data[24,44]. After filtering the iCLIP sites to alternative cassette exons and flanking introns, we searched for the YB-1 SELEX motifs (CATC and CACC) within 20 nucleotides upstream and downstream of the iCLIP sites.

1. Yang, X., Li, W., Prescott, E. D., Burden, S. J. & Wang, J. C. DNA topoisomerase II beta and neural development. *Science* **287**, 131–134 (2000).
2. Yang, X. *et al.* Patterning of muscle acetylcholine receptor gene expression in the absence of motor innervation. *Neuron* **30**, 399–410 (2001).
3. Lin, W. *et al.* Distinct roles of nerve and muscle in postsynaptic differentiation of the neuromuscular synapse. *Nature* **410**, 1057–1064 (2001).
4. Arber, S., Burden, S. J. & Harris, A. J. Patterning of skeletal muscle. *Curr Opin Neurobiol* **12**, 100–103 (2002).
5. Panzer, J. A., Song, Y. & Balice-Gordon, R. J. In vivo imaging of preferential motor axon outgrowth to and synaptogenesis at prepatterned acetylcholine receptor clusters in embryonic zebrafish skeletal muscle. *J Neurosci* **26**, 934–947 (2006).
6. Kim, N. & Burden, S. J. MuSK controls where motor axons grow and form synapses. *Nat Neurosci* **11**, 19–27 (2008).
7. Kim, N. *et al.* Lrp4 is a receptor for Agrin and forms a complex with MuSK. *Cell* **135**, 334–342 (2008).
8. Zhang, B. *et al.* LRP4 serves as a coreceptor of agrin. *Neuron* **60**, 285–297 (2008).
9. Zhang, W., Coldefy, A. S., Hubbard, S. R. & Burden, S. J. Agrin binds to the N-terminal region of Lrp4 protein and stimulates association between Lrp4 and the first immunoglobulin-like domain in muscle-specific kinase (MuSK). *J Biol Chem* **286**, 40624–40630 (2011).
10. Masiakowski, P. & Yancopoulos, G. D. The Wnt receptor CRD domain is also found in MuSK and related orphan receptor tyrosine kinases. *Curr Biol* **8**, R407–R407 (1998).
11. Xu, Y. K. & Nusse, R. The Frizzled CRD domain is conserved in diverse proteins including several receptor tyrosine kinases. *Curr Biol* **8**, R405–R406 (1998).
12. Stiegler, A. L., Burden, S. J. & Hubbard, S. R. Crystal structure of the frizzled-like cysteine-rich domain of the receptor tyrosine kinase MuSK. *J Mol Biol* **393**, 1–9 (2009).
13. Roszmusz, E., Patthy, A., Trexler, M. & Patthy, L. Localization of disulfide bonds in the frizzled module of Ror1 receptor tyrosine kinase. *J Biol Chem* **276**, 18485–18490 (2001).
14. Jennings, C. G., Dyer, S. M. & Burden, S. J. Muscle-specific trk-related receptor with a kringle domain defines a distinct class of receptor tyrosine kinases. *Proc Natl Acad Sci U S A* **90**, 2895–2899 (1993).
15. Valenzuela, D. M. *et al.* Receptor Tyrosine Kinase Specific for the Skeletal-Muscle Lineage - Expression in Embryonic Muscle, at the Neuromuscular-Junction, and after Injury. *Neuron* **15**, 573–584 (1995).
16. Zhang, B. *et al.* Wnt proteins regulate acetylcholine receptor clustering in muscle cells. *Mol Brain* **5**, 7 (2012).
17. Strochlic, L. *et al.* Wnt4 participates in the formation of vertebrate neuromuscular junction. *PLoS One* **7**, e29976 (2012).
18. Jing, L., Lefebvre, J. L., Gordon, L. R. & Granato, M. Wnt signals organize synaptic prepattern and axon guidance through the zebrafish unplugged/MuSK receptor. *Neuron* **61**, 721–733 (2009).
19. Gordon, L. R., Gribble, K. D., Syrett, C. M. & Granato, M. Initiation of synapse formation by Wnt-induced MuSK endocytosis. *Development* **139**, 1023–1033 (2012).
20. Jing, L., Gordon, L. R., Shtibin, E. & Granato, M. Temporal and spatial requirements of unplugged/MuSK function during zebrafish neuromuscular development. *PLoS One* **5**, e8843 (2010).
21. Zhang, J., Lefebvre, J. L., Zhao, S. & Granato, M. Zebrafish unplugged reveals a role for muscle-specific kinase homologs in axonal pathway choice. *Nat Neurosci* **7**, 1303–1309 (2004).
22. Zhou, H., Glass, D. J., Yancopoulos, G. D. & Sanes, J. R. Distinct domains of MuSK mediate its abilities to induce and to associate with postsynaptic specializations. *J Cell Biol* **146**, 1133–1146 (1999).
23. Antolik, C., Catino, D. H., Resneck, W. G. & Bloch, R. J. The tetratricopeptide repeat domains of rapsyn bind directly to cytoplasmic sequences of the muscle-specific kinase. *Neuroscience* **141**, 87–100 (2006).
24. Zarnack, K. *et al.* Direct competition between hnRNP C and U2AF65 protects the transcriptome from the exonization of Alu elements. *Cell* **152**, 453–466 (2013).
25. Shetty, S. Regulation of urokinase receptor mRNA stability by hnRNP C in lung epithelial cells. *Mol Cell Biochem* **272**, 107–118 (2005).
26. Lee, E. K. *et al.* hnRNP C promotes APP translation by competing with FMRP for APP mRNA recruitment to P bodies. *Nat Struct Mol Biol* **17**, 732–739 (2010).
27. McCloskey, A., Taniguchi, I., Shinmyozu, K. & Ohno, M. hnRNP C tetramer measures RNA length to classify RNA polymerase II transcripts for export. *Science* **335**, 1643–1646 (2012).
28. Kohno, K., Izumi, H., Uchiumi, T., Ashizuka, M. & Kuwano, M. The pleiotropic functions of the Y-box-binding protein, YB-1. *Bioessays* **25**, 691–698 (2003).
29. Wei, W. J. *et al.* YB-1 binds to CAUC motifs and stimulates exon inclusion by enhancing the recruitment of U2AF to weak polypyrimidine tracts. *Nucleic Acids Res* **40**, 8622–8636 (2012).
30. Hung, L. H. *et al.* Diverse roles of hnRNP L in mammalian mRNA processing: a combined microarray and RNAi analysis. *RNA* **14**, 284–296 (2008).
31. Rossbach, O. *et al.* Crosslinking-immunoprecipitation (iCLIP) analysis reveals global regulatory roles of hnRNP L. *RNA Biol* **11**, 146–155 (2014).
32. Hui, J. *et al.* Intronic CA-repeat and CA-rich elements: a new class of regulators of mammalian alternative splicing. *EMBO J* **24**, 1988–1998 (2005).
33. Hui, J., Stangl, K., Lane, W. S. & Bindereif, A. HnRNP L stimulates splicing of the eNOS gene by binding to variable-length CA repeats. *Nat Struct Biol* **10**, 33–37 (2003).
34. Chiou, N. T., Shankarling, G. & Lynch, K. W. hnRNP L and hnRNP A1 induce extended U1 snRNA interactions with an exon to repress spliceosome assembly. *Mol Cell* **49**, 972–982 (2013).
35. House, A. E. & Lynch, K. W. An exonic splicing silencer represses spliceosome assembly after ATP-dependent exon recognition. *Nat Struct Mol Biol* **13**, 937–944 (2006).
36. Motta-Mena, L. B., Heyd, F. & Lynch, K. W. Context-dependent regulatory mechanism of the splicing factor hnRNP L. *Mol Cell* **37**, 223–234 (2010).
37. Tong, A., Nguyen, J. & Lynch, K. W. Differential expression of CD45 isoforms is controlled by the combined activity of basal and inducible splicing-regulatory elements in each of the variable exons. *J Biol Chem* **280**, 38297–38304 (2005).
38. Rahman, M. A. *et al.* HnRNP L and hnRNP LL antagonistically modulate PTB-mediated splicing suppression of CHRNA1 pre-mRNA. *Sci Rep* **3**, 2931 (2013).
39. Guang, S., Felthauser, A. M. & Mertz, J. E. Binding of hnRNP L to the pre-mRNA processing enhancer of the herpes simplex virus thymidine kinase gene enhances both polyadenylation and nucleocytoplasmic export of intronless mRNAs. *Mol Cell Biol* **25**, 6303–6313 (2005).
40. Hui, J., Reither, G. & Bindereif, A. Novel functional role of CA repeats and hnRNP L in RNA stability. *RNA* **9**, 931–936 (2003).
41. Masuda, A. *et al.* hnRNP H enhances skipping of a nonfunctional exon P3A in CHRNA1 and a mutation disrupting its binding causes congenital myasthenic syndrome. *Hum Mol Genet* **17**, 4022–4035 (2008).
42. Schaal, T. D. & Maniatis, T. Multiple distinct splicing enhancers in the protein-coding sequences of a constitutively spliced pre-mRNA. *Mol Cell Biol* **19**, 261–273 (1999).
43. Black, D. L. Mechanisms of alternative pre-messenger RNA splicing. *Annu Rev Biochem* **72**, 291–336 (2003).
44. Konig, J. *et al.* iCLIP reveals the function of hnRNP particles in splicing at individual nucleotide resolution. *Nat Struct Mol Biol* **17**, 909–915 (2010).
45. Wang, Y. *et al.* A complex network of factors with overlapping affinities represses splicing through intronic elements. *Nat Struct Mol Biol* **20**, 36–45 (2013).
46. Rideau, A. P. *et al.* A peptide motif in Raver1 mediates splicing repression by interaction with the PTB RRM2 domain. *Nat Struct Mol Biol* **13**, 839–848 (2006).
47. Bland, C. S. *et al.* Global regulation of alternative splicing during myogenic differentiation. *Nucleic Acids Res* **38**, 7651–7664 (2010).
48. Song, Y. J. & Lee, H. YB1/p32, a nuclear Y-box binding protein 1, is a novel regulator of myoblast differentiation that interacts with Msx1 homeoprotein. *Exp Cell Res* **316**, 517–529 (2010).
49. Bian, Y. *et al.* Tannic acid facilitates expression of the polypyrimidine tract binding protein and alleviates deleterious inclusion of CHRNA1 exon P3A due to an hnRNP H-disrupting mutation in congenital myasthenic syndrome. *Hum Mol Genet* **18**, 1229–1237 (2009).
50. Koike, S., Schaeffer, L. & Changeux, J. P. Identification of a DNA element determining synaptic expression of the mouse acetylcholine receptor delta-subunit gene. *Proc Natl Acad Sci U S A* **92**, 10624–10628 (1995).
51. Duclert, A., Savatier, N., Schaeffer, L. & Changeux, J. P. Identification of an element crucial for the sub-synaptic expression of the acetylcholine receptor epsilon-subunit gene. *J Biol Chem* **271**, 17433–17438 (1996).
52. Ohno, K., Anlar, B. & Engel, A. G. Congenital myasthenic syndrome caused by a mutation in the Ets-binding site of the promoter region of the acetylcholine receptor epsilon subunit gene. *Neuromuscul Disord* **9**, 131–135 (1999).
53. Lee, H. H. *et al.* Transcriptional regulation of acetylcholinesterase-associated collagen ColQ: differential expression in fast and slow twitch muscle fibers is driven by distinct promoters. *J Biol Chem* **279**, 27098–27107 (2004).
54. Shiomi, K. *et al.* CDK4 and cyclin D1 allow human myogenic cells to recapture growth property without compromising differentiation potential. *Gene Ther* **18**, 857–866 (2011).
55. Wada, M. R., Inagawa-Ogashiwa, M., Shimizu, S., Yasumoto, S. & Hashimoto, N. Generation of different fates from multipotent muscle stem cells. *Development* **129**, 2987–2995 (2002).
56. Hashimoto, N. *et al.* Immortalization of human myogenic progenitor cell clone retaining multipotentiality. *Biochem Biophys Res Commun* **348**, 1383–1388 (2006).

57. Ohno, K. *et al.* Myasthenic syndromes in Turkish kinships due to mutations in the acetylcholine receptor. *Ann Neurol* **44**, 234–241 (1998).
58. Mayeda, A. & Krainer, A. R. Mammalian in vitro splicing assays. *Methods Mol Biol* **118**, 315–321 (1999).
59. Shiota, M. *et al.* Y-box binding protein-1 promotes castration-resistant prostate cancer growth via androgen receptor expression. *Endocr Relat Cancer* **18**, 505–517 (2011).
60. Chao, J. A., Patskovsky, Y., Almo, S. C. & Singer, R. H. Structural basis for the coevolution of a viral RNA-protein complex. *Nat Struct Mol Biol* **15**, 103–105 (2008).

Acknowledgments

We are grateful to Dr. Akira Yokomizo (Kyushu University, Japan) for providing pCMV-YB-1-myc-nuc expression vector, to Dr. Naohiro Hashimoto (National Center for Geriatrics and Gerontology, Japan) for providing KD3 cells, and to Dr. Kentaro Taki (Nagoya University) for technical assistance on the mass spectrometry analysis. This work was supported by Grants-in-Aid from the MEXT and MHLW of Japan.

Author contributions

Ki.O. conceived the project. F.N., M.A.R. and A.M. designed experiments; F.N. performed most of the experiments; M.A.R. contributed to RNA affinity purification assay and mass spectrometry analysis; Ke.O. and J.T. contributed to RNA-EMSA and *in silico* analysis, respectively. F.N., M.A.R. and Ki.O. wrote the paper.

Additional information

Supplementary information accompanies this paper at http://www.nature.com/scientificreports

Competing financial interests: The authors declare no competing financial interests.

How to cite this article: Nasrin, F. *et al.* HnRNP C, YB-1 and hnRNP L coordinately enhance skipping of human *MUSK* exon 10 to generate a Wnt-insensitive MuSK isoform. *Sci. Rep.* 4, 6841; DOI:10.1038/srep06841 (2014).

J Orthop Sci (2014) 19:827–831
DOI 10.1007/s00776-014-0595-2

ORIGINAL ARTICLE

Skeletal complications in congenital insensitivity to pain with anhidrosis: a case series of 14 patients and review of articles published in Japanese

Yasu Zhang · Nobuhiko Haga

Received: 27 December 2013 / Accepted: 1 May 2014 / Published online: 23 June 2014

Abstract
Background Congenital insensitivity to pain with anhidrosis (CIPA) is a rare disorder with various skeletal complications; thus, a compilation of data on affected patients could provide a valuable resource for the management of this disease. The aim of this study was to ascertain and report the frequency, location, age of onset, cause, and management of skeletal complications in Japanese patients with CIPA.
Methods The medical records of 14 CIPA patients in our institute and information on 77 patients reported in Japanese articles were analyzed. Data regarding skeletal-system complications, including location, symptom, major cause and management of fractures, joint dislocations, infections, and Charcot joints, were extracted.
Results Fractures occurred in 59/91 patients (65 %), 91 % of them in the lower limbs. Joint dislocations occurred in 27/91 patients (30 %), 91 % of them in the hip joint. Bone and joint infections occurred in 22 patients (24 %) and Charcot joints in 26 patients (29 %); 62 % of infections and 87 % of Charcot joints developed in the lower limbs. Most fractures occurred from 1 to 7 years of age; there was no apparent relationship between age and other complications. The major known causes of bone disorders were minor trauma such as short falls; however, most were of unknown cause. Conservative therapy was used more frequently than surgery to manage fractures, dislocations, and Charcot joints.
Conclusions These data show that most CIPA patients have skeletal complications, most of which occur in the lower limbs. Fractures are frequent between 1 and 7 years of age, whereas other bone disorders have no apparent age relationship. The major known causes of bone disorders were minor trauma such as short falls. Conservative therapy was more frequently used to manage fractures, dislocations, and Charcot joints.

Introduction

Hereditary sensory and autonomic neuropathies (HSAN), a group of disorders characterized by insensitivity to noxious stimuli and autonomic dysfunction, are associated with pathological abnormalities of the peripheral nerves. Dyck [1] identified five types; HSAN type VI was added recently [2]. HSAN type IV, also called congenital insensitivity to pain with anhidrosis (CIPA), is an autosomal recessive disorder associated with mutation of the *NTRK1* gene, which codes for neurotrophic tyrosine kinase [3]. CIPA is characterized by absence of pain sensation, anhidrosis, episodes of recurrent fever, intellectual disability, and self-mutilating behavior [4, 5].

Pain sensation is a body alarm signal. Without it, there is a lack of protective reactions to acute pain. Therefore, individuals with CIPA may sustain repeated bone fractures and multiple joint dislocations [6–9]. In addition, patients often do not realize that they have injuries, which leads to delays in diagnosis and difficulties with treatment. Intellectual disability and self-mutilating behavior can lead to slow healing of such injuries, resulting in limb deformities and Charcot joints. Consequently, many adult patients cannot walk independently and require wheelchairs. High thresholds for perception of touch/pressure and deep

Y. Zhang · N. Haga (✉)
Department of Rehabilitation Medicine, Graduate School of Medicine, The University of Tokyo, 7-3-1 Hongo, Bunkyo-ku, Tokyo 113-8655, Japan
e-mail: hagan-reh@h.u-tokyo.ac.jp

sensations [10] can also adversely affect skeletal complications. In patients with CIPA, intellectual disability includes speech delay, communication disorder, and attention deficit hyperactivity disorder. Common self-mutilating behavior is biting one's own tongue, lips, and fingertips.

Certain geographical areas, including Israel [11, 12] and Japan, have a relatively higher prevalence of this disease. The number of Japanese patients is estimated at 130–210 [13]; thus, the prevalence in Japan is believed to be higher than in Western countries. Although many CIPA patients have been described in previously published Japanese reports, there are no objective reports on skeletal disorders in a series of patients. Thus, a compilation of data on Japanese patients with CIPA could provide a valuable resource for management of this disease. The aim of this study was thus to ascertain and report the frequency, location, age of onset, cause, and management of skeletal complications in Japanese patients with CIPA.

Patients and methods

The medical records of 14 CIPA patients followed up by the Department of Rehabilitation Medicine, the University of Tokyo Hospital, between January 2008 and December 2011 were collected [patient records group (PRG)]. Diagnoses of all these patients were based on clinical findings and physiological tests. Gene analyses on three of them showed *NTRK1* mutations. Case reports and case series of CIPA written in Japanese were collected as follows: The Japanese language medical literature database (Ichushi WEB) was searched using the keywords sentensei mutsuumukanshou (congenital insensitivity to pain with anhidrosis), mutsuu mukan (insensitivity to pain, anhidrosis), mukan mutsuu (anhidrosis, insensitivity to pain), and mutsuumukanshou (insensitivity to pain with anhidrosis). All Japanese articles between January 1983 and December 2011 were assessed, and case reports and case series about patients with CIPA were selected for this review. When two articles dealing with a single patient were identified, the more recent one was primarily used while also accessing information from the original one. Seventy-six articles reporting 77 patients with clinically proven CIPA [literature review group (LRG)], six of whom reportedly had the *NTRK1* mutation, were reviewed.

For both PRG and LRG, sex, age (PRG at last visit, LRG at time of report), and presence of intellectual disability were surveyed. Data regarding skeletal complications, classified as fractures, joint dislocations, infections (pyogenic osteomyelitis and arthritis), and Charcot joints in the extremities and trunk, were extracted. Extracted information included age at occurrence of skeletal complication, location, symptoms, major causes, and management. Because some patients had multiple locations or symptoms, each occurrence of a skeletal complication was assessed separately.

This study was approved by the ethical committee of the Faculty of Medicine, the University of Tokyo (approval number 2373).

Results

Patient data

General data, including sex, age, duration of follow-up, and presence/absence of intellectual disability, are listed in Table 1. The median age in the LRG was younger than that in the PRG. There were no differences between groups in sex or presence of intellectual disability.

Table 1 Patient data

	Total	PRG	LRG
Number of patients	91	14	77
Male/female/not documented	41/49/1	7/7/0	34/42/1
Age (years)[a]	11 (0–37)	14 (4–35)	11 (0–37)
Duration of follow-up (months)[a]	Not applicable	30 (3–46)	Not applicable
With intellectual disability/ without/not documented	55/11/25	10/3/1	45/8/24

LRG literature review group, *PRG* patient records group

[a] Median (range)

Table 2 Locations of fractures and dislocations

	Total	PRG (14 patients)	LRG (77 patients)
Fractures	116	32	84
Clavicle	2	2	None
Upper arm	2	1	1
Elbow	2	2	None
Forearm	5	None	5
Hip	2	None	2
Thigh	26	6	20
Knee	7	3	4
Lower leg	35	6	29
Foot	35	12	23
Dislocations	33	18	15
Shoulder	2	1	1
Hip	30	17	13
Foot	1	None	1

LRG literature review group, *PRG* patient records group

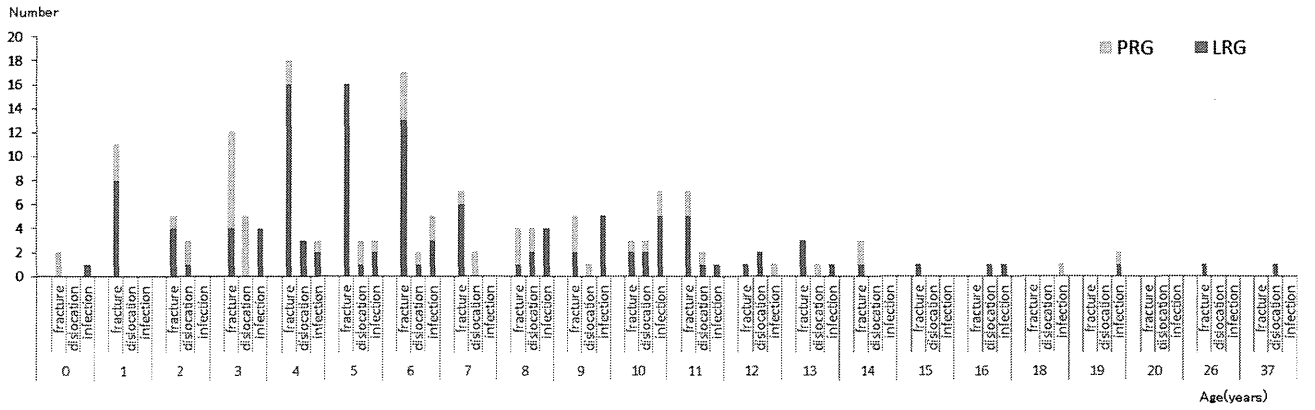

Fig. 1 Onset age of fractures, dislocations, and infections for patient records group (PRG) and for literature review group (LRG)

Data on skeletal complications

Fractures

In all, 116 fractures were analyzed; 105 (91 %) were in the lower limbs. Most lower-limb fractures occurred in the lower leg and foot (Table 2). Fractures were frequent between the ages of 1 and 7 years, especially between the ages of 4 and 6 years (Fig. 1).

Documented causes of fractures included falls (nine), minor external force (six), jumping from a step (four), abnormal gait (two), motor vehicle accident (one), and no specific reason (seven); causes of the other 87 fractures were not clearly described. Thirteen of 116 fractures (11 %) were managed surgically and 47 of 116 (41 %) conservatively; for the other 56 fractures, management was not documented. Surgical management for 13 fractures led to breakage or dislodgement of the fixation implant in five instances and surgical-site infection in three; conservative management for 47 fractures led to pressure-sore formation in three.

Joint dislocations

In all, 33 joint dislocations were analyzed: 30 of the 33 (91 %) occurred in the hip joint (Table 2). There was no apparent relationship with age (Fig. 1). Causes of joint dislocations included falls (one), abnormal gait (one), external force (one), and changing a diaper (one); for the other 29 dislocations, causes were not clearly documented. Three of 33 joint dislocations (9 %) were managed surgically and eight (24 %) conservatively; for the other 22, management was not documented.

Infections

In all, 39 infections were analyzed. Twenty-four presented as osteomyelitis and 15 as arthritis. Twenty-four of 39 (62 %) occurred in the lower limbs (Table 3). Though biting one's own fingertips was reported in eight patients, no osteomyelitis or arthritis caused by this was reported. There was no apparent relationship with age (Fig. 1). Seventeen of 39 infections (44 %) were managed surgically, and six (15 %) were managed conservatively; for the other 16 infections, management was not documented.

Table 3 Locations of infections and Charcot joints

	Total	PRG (14 patients)	LRG (77 patients)
Infections	39	9	30
Upper limb	15	3	12
Lower limb	24	6	18
Charcot joints	52	15	37
Elbow	3	2	1
Hip	12	2	10
Knee	16	5	11
Ankle	17	5	12
Spine	4	1	3

LRG literature review group, *PRG* patient records group

Charcot joints

In all, 52 Charcot joints were analyzed. Forty-five (87 %) occurred in the lower limbs (Table 3); 4/52 (8 %) were managed surgically, and 8/52 (15 %) were managed conservatively; for the other 40, management was not documented.

Multiple and/or repeated musculoskeletal conditions

Among the 14 patients in PRG, two experienced multiple and/or repeated musculoskeletal conditions during the follow-up period of 4 years. A 3-year-old girl developed left hip dislocation that recurred 17 times during the